# NUMERICAL SIMULATION OF LIQUID-SOLID SLURRY FLOW USING THE EULERIAN-EULERIAN TWO-FLUID MODEL

A Thesis Submitted to the
College of Graduate and Postdoctoral Studies
In Partial Fulfillment of the Requirements for the Degree of
**Master of Science**
In the Department of Mechanical Engineering
University of Saskatchewan
Saskatoon

By

**Omar Renzo Piminchumo Marinos**

## PERMISSION TO USE

In presenting this thesis in partial fulfilment of the requirements for a Postgraduate degree from the University of Saskatchewan, I agree that the Libraries of this University may make it freely available for inspection. I further agree that permission for copying of this thesis in any manner, in whole or in part, for scholarly purposes may be granted by the professor or professors who supervised my thesis work or, in their absence, by the Head of the Department or the Dean of the College in which my thesis work was done. It is understood that any copying or publication or use of this thesis or parts thereof for financial gain shall not be allowed without my written permission. It is also understood that due recognition shall be given to me and to the University of Saskatchewan in any scholarly use which may be made of any material in my thesis.

Requests for permission to copy or to make other use of material in this thesis in whole or part should be addressed to:

Head of the Department of Mechanical Engineering
University of Saskatchewan
Engineering Building, 57 Campus Drive
Saskatoon, Saskatchewan S7N 5A9 Canada

or

Dean
College of Graduate and Postdoctoral Studies
University of Saskatchewan
116 Thorvaldson Building, 110 Science Place
Saskatoon, Saskatchewan S7N 5C9 Canada

## ABSTRACT

A numerical study was conducted to assess the performance of a Two-Fluid Model (TFM) developed for gas-solid flow in predicting liquid-solid flow, as well as a TFM specifically modified for liquid-solid flow. The physics involved in gas-solid and liquid-solid flows are intuitively different, and some model terms that can be neglected in a gas-solid formulation turn out to be highly relevant in liquid-solid flow. The difference in these two flows is partly due to the fact that the most important physical properties of the fluid, e.g., density and dynamic viscosity, are much higher in a liquid compared to a gas. In order to investigate the differences between the two base case models, three intermediate models were proposed, and together with the two base case models, assessed in terms of their predictions for an experimental test case. The specific test case was fully developed, turbulent, steady flow of a liquid solid mixture in a vertical pipe. The main differences in the model formulations pertain to the fluid momentum, granular temperature and turbulence kinetic energy transport equations. The other model terms remained similar, i.e., the eddy viscosity constitutive relation, the LRN $k-\varepsilon$ closure and the turbulence modulation relations. The present study focused on the predictions for the velocity profile of both the liquid and solid phases, the solids volume fraction profile and budgets of the transport equations for the granular temperature and turbulence kinetic energy. The results obtained were used to identify the model terms that are most significant. These include new formulations for the solids viscosity and granular temperature conductive coefficient, which include the effects of the interstitial fluid effect. The single most important term was the model for the long-range particle fluctuations through the fluid, which played a dominant role in the balance of the turbulence kinetic energy and granular temperature transport equations. The present thesis proposes that this term, which was specifically developed for the case of liquid-solid flow, should be configured as a sink term in the granular temperature equation and a source term in the turbulence kinetic energy equation. With this modification, the numerical predictions were much closer to the experimental data, especially in terms of the solids volume fraction profile in the near-wall region.

## ACKNOWLEDGEMENT

I would like to thank Professor Donald J. Bergstrom for allowing me to join his research group and guide my steps with wisdom, motivation and patience until I reach the culmination of the Master's program and make a significant contribution through the present thesis work.

I would like to express my acknowledgement to my advisory committee members Prof. Jim Bugg and Prof. Richard Evitts for their contributions to this work through their effective observations and recommendations.

I would also like to thank the CFD research group for their continued support and assistance throughout the program, as well as other colleagues at the Department of Mechanical Engineering and the College and Engineering for their kind and sincere friendship. I would like to express a special acknowledgment to Shawn Reinink for his valuable guidance and support in different aspect of my graduate studies.

## DEDICATION

To
My wonderful parents Natalia and Miguel;
my wife Fatima, my sister Lorena,
and my lovely daughter Sofia.

## TABLE OF CONTENTS

## LIST OF TABLES

## LIST OF FIGURES

## LIST OF SYMBOLS

### Acronyms

| | |
|---|---|
| CFD | Computational Fluid Dynamics |
| DEM | Discrete Element Simulation |
| DNS | Direct Numerical Simulation |
| LES | Large Eddy Simulation |
| LDV | Laser Doppler Velocimetry |
| RANS | Reynolds Averaged Navier-Stokes |
| SRC | Saskatchewan Research Council |

### Nomenclature

| | |
|---|---|
| $A$ | Cross-sectional area of pipe [$m^2$] |
| $C_\mu$,$C_{\varepsilon 1}$, $C_{\varepsilon 2}$,$C_{\varepsilon 3}$ | Low Reynolds Number model constants |
| $C_D$ | Drag coefficient |
| $C_W$ | Parameter in $E_W$ |
| $d_P$ | Particle diameter [mm] |
| $D$ | Pipe diameter [mm] |
| $D_r = \rho_s/\rho_f$ | Density ratio |
| $e$,$e_s$,$e_f$ | Coefficient of restitution in regular model, vacuum conditions and interstitial effect |
| $e_w$ | Coefficient of restitution at wall |
| $E_W$ | Enhancement of turbulent kinetic energy due wakes [$kgm^{-1}s^{-2}$] |
| $f_{12}$ | Interfacial friction factor |
| $f$ | Friction factor |
| $f_\mu$,$f_1$, $f_2$ | Low Reynolds Number model functions |
| $F_i$ | External force on particle per unit mass [$ms^{-2}$] |
| $F_d$ | Drag force [N] |
| $g$ | Gravitational acceleration [$ms^{-2}$] |
| $g_o$ | Radial distribution function |

| | |
|---|---|
| $G_k$ | Functional relations related to kinetic theory models, k = 1,2,3,4 |
| $G_{1k}$,$G_{2k}$, $G_{3k}$ | Particle stress kinetic contributions |
| $G_{1c}$,$G_{2c}$, $G_{3c}$ | Particle stress collisional contributions |
| $I_k$ | Turbulence modulation in turbulence kinetic energy equation [$kgm^{-1}s^{-2}$] |
| $I_T$ | Turbulence modulation for granular temperature [$kgm^{-1}s^{-2}$] |
| $J_L$ | Fluid superficial velocity [$ms^{-1}$] |
| $J_S$ | Solid superficial velocity [$ms^{-1}$] |
| $k$ | Turbulence kinetic energy [$m^2s^{-2}$] |
| $m$ | Mass loading |
| $M_k$ | Momentum inter-phase drag transfer [N] |
| $n$ | Outward pointing normal |
| $P$ | Pressure [Pa] |
| $P_k$ | Production term due to shear in fluid phase [$kgm^{-1}s^{-2}$] |
| $P_T$ | Granular Temperature production term [$kgm^{-1}s^{-2}$] |
| $q_{PTr}$ | Granular temperature conduction [$kgs^{-3}$] |
| $R_p$ | Particle Reynolds Number |
| $r$ | Radial coordinate [m] |
| $S_{sij}$ | Solid strain rate tensor [$s^{-1}$] |
| $S_{fij}$ | Fluid-solids strain rate tensor [$s^{-1}$] |
| $S_T = \tau_P/\tau_f$ | Stokes number |
| $t$ | Time [s] |
| $T$ | Granular temperature [$m^2s^{-2}$] |
| $u$, $v$ | Instantaneous fluid and solid velocity field [$ms^{-1}$] |
| $u'$,$v'$ | Fluid and solids velocity fluctuation [$ms^{-1}$] |
| $u_\tau$ | Friction velocity [$ms^{-1}$] |
| $u^+$ | Mean velocity in inner units, $u/u_\tau$ |
| $U$, $V$ | Mean Fluid and solid bulk velocity [$ms^{-1}$] |
| $U_r$ | Mean relative velocity [$ms^{-1}$] |
| $\overline{u_i'v_i'}$ | Variance of solid and fluid velocity fluctuations [$m^2s^{-2}$] |
| V | Characteristic control volume [$m^3$] |

| | |
|---|---|
| $w$ | Total mass flow rate [$kgs^{-1}$] |
| $x, y, z$ | Cartesian coordinates in the streamwise, wall-normal or cross-stream direction |
| $r, \theta, z$ | Cylindrical coordinates in the axial, wall-normal or cross-stream direction |

**Greek Symbols**

| | |
|---|---|
| $\alpha_f$ | Liquid phase volume fraction |
| $\alpha_s$ | Solids phase volume fraction |
| $\alpha_o$ | Solids maximum volume fraction |
| $\beta$ | Inter-phase drag function [$kgm^3s$] |
| $\gamma$ | Dissipation rate of granular temperature due particles collision [$kgms^3$] |
| $\varepsilon$ | Dissipation rate of turbulent kinetic energy [$m^2s^{-3}$] |
| $\rho$ | Density [$kgm^{-3}$] |
| $\mu$ | Dynamic viscosity [$kgm^{-1}s^{-1}$] |
| $\nu$ | Kinematic viscosity [$m^2s^{-1}$] |
| $\lambda$ | Diffusion coefficient of granular temperature [$kgm^{-1}s^{-1}$] |
| $\tau_{sij}$ | Solids phase effective stress tensor [$kgm^{-1}s^{-2}$] |
| $\tau_{fij}$ | Fluid phase effective stress tensor [$kgm^{-1}s^{-2}$] |
| $\tau_c$ | Particle-particle collision time [s] |
| $\tau_P$ | Particle response timescale [s] |
| $\tau_f$ | Flow field timescale [s] |
| $\tau_w$ | Wall shear stress [$kgm^{-1}s^{-2}$] |
| $\phi$ | Specularity coefficient |
| $\omega$ | Damping function |

**Subscripts**

| | |
|---|---|
| $coll$ | Collision |
| $f$ | Fluid phase |
| $l$ | Liquid phase |

| | |
|---|---|
| $m$ | Mixture |
| $s$ | Solid phase |
| $w$ | Wall |

**Superscripts**

| | |
|---|---|
| $+$ | Dimensionless indicator |
| $'$ | Fluctuating component of a variable |
| $*$ | Modified when interstitial fluid exists |

**Operators and special notations**

| | |
|---|---|
| $\Delta$ | Difference |
| $\partial/\partial t$ | Partial derivative |
| $D/Dt$ | Material derivative |

# Chapter 1: Introduction

## 1.1 Preliminaries

Multiphase flow refers to the mixing of at least two phases, such as liquid-solid, gas-solid, or liquid-gas flow. In oil production, a combination of liquid-solid-gas flow can occur because of the different components in crude oil and the temperature and composition of the reservoir. The presence of any of these phases may have severe consequences for the performance of production and transport equipment, e.g., erosion and sedimentation in pipes and pumps. In two-phase flows, the fluid phase is considered as the continuum or carrier phase, while the particulate phase is referred to as the dispersed phase. The study of this type of flow has become important due to its relevance in industrial applications, e.g., hydrotransport of minerals, fluidized beds, water purification, chemical reactors, oilfield production and pneumatic transport of particles in pipes, and its occurrence in natural processes, e.g., atmospheric dispersion and sediment transport. In this context, a better understanding of the underlying physics is required to improve our predictive capability.

In typical industrial applications, most flows are turbulent. There is an extensive literature on single-phase turbulence and various models exist to predict it, e.g., Pope (2000), Tennekes and Lumley (1972) and Wilcox (2002). To predict a turbulent flow field it is necessary to solve a set of partial differential equations, e.g., the Navier-Stokes equations, most often by the application of numerical methods, which is referred as Computational Fluid Dynamics (CFD). The complexity and detail of the final flow solution depends on the method adopted, e.g., Direct Numerical Simulation (DNS), Large Eddy Simulation (LES) or Reynolds Averaged Navier-Stokes (RANS) methods. DNS is able to model the complete details of a flow, but it is only

applicable to low Reynolds number flows due to the amount of computational resources required. LES uses less but still substantial resources to predict the large-scale motions. The RANS method requires the least computational resources, but only predicts the time-average or mean behavior of the flow field. One of the most popular turbulence closures for RANS is the $k-\varepsilon$ model, which relates the eddy viscosity to the turbulence kinetic energy $k$ and its dissipation rate $\varepsilon$. Both, $k$ and $\varepsilon$ are calculated from their respective transport equations. The application of RANS with a $k-\varepsilon$ model is frequently used to predict industrial flows.

The solid (or particle) phase has a strong influence on the fluid flow field, both in terms of the overall transport and the turbulence field. This influence becomes less important at low levels of the solid volume fraction; however, at moderate levels, particles begin to interact, which makes the process of modeling more complex. When the volume fraction increases to very high levels, the fluid turbulence may no longer exist. The current focus of engineers and physicists is to develop models that can simulate the important physical interactions of multiphase flow and obtain accurate predictions of the mean flow behavior. The successful application of CFD to two-phase flows requires a correct understanding of the physical mechanisms that affect the transport of these mixtures.

Experimental tests of liquid-solid flow have been documented by various studies, e.g., Sanders *et al*. (2000), Spelay *et al*. (2016) and Matoušek (2009). Unfortunately, this type of research usually demands high investment in facilities and instrumentation to measure specific properties of the flow. Laser Doppler Velocimetry (LDV) and Gamma-ray densitometer techniques are commonly used in experimental studies of multiphase flow. Due to the diverse combinations of particle diameter, pipe diameter, type of fluid, etc. that exist in industrial applications, to perform experimental studies of all cases is typically not feasible. A more practical approach for industry is the use of CFD. A validated CFD model provides the flexibility to evaluate a wide range of flow parameters. For the case of two-phase flow, both Eulerian-Lagrangian and Eulerian-Eulerian exist. The first method consists of following a particle along its trajectory through a specific domain. An advantage of this method is that closure models are not required. However, due to its nature, this method may not be appropriate for dense flows. The second method, also referred to as the two-fluid model, requires less

computational resources and can be applied to dense flow regimes. However, it introduces closure relations to solve different aspects of the flow. Unfortunately, a definitive formulation of this model, able to predict diverse types of two-phase flows, is still lacking.

### 1.2 Motivation

Solids transport by liquid in pipelines includes a wide variety of applications in the oil and gas sector, such as transport of oil sand, artificial lift production and drilling operations. In the paper manufacturing industry, hydro-transport of a mixture composed of water, chemicals and cellulose particles is used to achieve the large production volumes this industry requires. In order to obtain an effective design of liquid-solid flows, it is crucial to understand the physical principles involved in particle and liquid motion, and their interaction.

For numerical predictions, accurate implementation of the hydrodynamic forces affecting the particle motion, definition of the correct boundary conditions and selection of appropriate mathematical models represent the major challenges. At the most specific level of description, the particles are surrounded by a fluid, the flow field of which can be described by the well-known Navier-Stokes equations, and Newton's equation of motion can be used to predict the particle trajectory. Unfortunately, to implement this level of detail it would be necessary to solve the flow field at the smallest scales, representing an extensive computational load that might not be feasible. This task becomes even more demanding for the high Reynolds number flows with a large number of particles. The TFM represents an alternative solution to this problem; it describes the particle flow in terms of the continuum-like properties. The TFM equations are derived by applying an averaging procedure. This process generates additional terms, related mostly to the fluctuating velocity component of the particle flow field and the fluid-particle interactions. The most common averaging techniques reported in the literature include time averaging (Ishii, 1975), volume averaging (Drew, 1983, Brennen, 2005) and ensemble averaging (Hiltunen *et al*., 2009). No matter the type of averaging, the final transport equations are very similar, with temporal, convective, diffusive and source terms: the major differences relate to the source terms, e.g., the hydrodynamic force. One of the most widely referenced set of equations were proposed by Anderson and Jackson (1967), who derived a set

of local averaged equations by applying a weighting function to the Navier-Stokes equations and the equation of motion for a particle.

Overall, the TFM represents a group of equations for solving the mean liquid and particle velocity fields. The complexity of the numerical solution pertains to the additional terms produced by the averaging procedure related to the fluctuations of the velocity fields and the particle-fluid interactions. For example, to solve the fluctuating velocity of the fluid phase, a set of turbulence models have been proposed in the literature. However, the presence of particles in the flow affects the turbulence of the fluid phase, which can be either enhanced or attenuated. This effect is referred to as turbulence modulation and different models to predict it can be found in the literature. Likewise, the dispersed phase requires additional theoretical assumptions and formulations. One approach for the particle phase is to apply the kinetic theory of gases to the solid particles, as if they were molecules. This approach yields an additional set of differential equations that allows the dispersed phase properties such as particle viscosity, particle pressure, particle velocity and volume fraction to be solved as functions of a new variable that characterizes the particle fluctuations, i.e., the granular temperature. This theory is known as the Kinetic Theory of Granular Flow (KTGF), and has been relatively successful in predicting gas-solid flows. However, the application of this theory to liquid-solid flow is still limited, since it involves additional physical considerations that can be neglected in gas-solid flows, e.g., the effect of the interstitial fluid. The KTGF was initially derived by considering particles moving in a vacuum, which is not a very realistic assumption when the gas is replaced by a liquid as the carrier phase. As such, the TFM combined with the KTGF is still in some ways unsatisfactory for the prediction of liquid-solid flows. The present research is focused on improving the simulation of liquid-solid flow using this method.

### 1.3 Challenges and Objectives

CFD represents a potentially useful methodology for predicting multiphase flow. CFD tools have provided accurate approximations for gas-particle flows, e.g., pipe flow and fluidized bed applications, based on comparison to the available experimental data. Extensive research exists

for gas-solid flow, however this is not the case for liquid-solid flow, especially for vertical flow in a pipe. The development of a definitive TFM formulation that includes the relevant physics, e.g, interstitial fluid effects, is still a work in progress.

The first challenge to developing a realistic model for liquid-solid flow using the Eulerian-Eulerian TFM and KTGF is the derivation of the appropriate constitutive equations and boundary conditions. Typically the constitutive equations used to model liquid-solid flows are the same as those used to predict gas-solid flows. This is likely not an accurate assumption given that the interstitial effect of the liquid is much higher compared to a gas, so that the particle phase properties may change considerably. In addition, when liquid is the carrier phase, additional forces become important. For example, the added mass or virtual mass force becomes important for flows with low density ratios (particle density/fluid density).

To achieve accurate predictions for liquid–solid multiphase flows requires a clear understanding of the complex interaction between the fluid and solid phases. The source and sink terms in the mean and turbulence transport equations, and some of the flow properties change due interstitial effects. In addition, the standard TFM and KTGF constitutive equations are formulated for the dispersed flow regime, when the bulk solid volume fraction is less than 5%. Additional effects for the solid phase occur when the volume fraction of the solid particles is in the dense flow regime, i.e., frictional forces appear as a new source of momentum transfer between particles, which requires that the constitutive equations be modified to include this behavior. For the present research the dense regime is not considered and thus the frictional component is not included.

Finally, most of the liquid-solid flow experimental studies available in literature relate to horizontal flows, whereas only a few of them focus on vertical pipe flow. One reason could be that most industrial applications involve horizontal pipes. Horizontal flow involves additional features in the solid phase transport equations, i.e., the effect of gravity on the radial velocity component, which generates an asymmetry of the solids phase flow. In contrast, vertical flow offers the advantage of an axisymmetric flow for both phases, fluid and solid. It can be studied

in the context of a fully-developed flow configuration, which facilitates the numerical implementation and allows a clearer picture of different modeling features, such as the effect of the interstitial fluid.

In response to the challenges described above, the present thesis research addresses the following objectives:

1. **Perform an extensive literature review of the constitutive equations and experimental studies of liquid-solid flow:** The standard form of the TFM and KTGF models neglects the effect of the interstitial fluid. To explore the interstitial fluid effect, a recent model for a liquid-solid flow is identified in the literature and used for the present computational study. In addition, an appropriate experimental database is selected to document dispersed liquid-solid upward flow in a vertical pipe.

2. **To reconfigure an in-house code for simulation liquid-solid flow in a vertical pipe:** An existing in-house CFD code developed in Fortran, and used by previous students to perform numerical simulations of turbulent gas-solid flow, is modified to consider liquid-solid flow. This code uses the Finite Volume Method to discretize and solve a set of transport equations.

3. **To perform a comprehensive analysis of the performance of the TFM for liquid-solid flow:** Five different TFM formulations are analyzed based on comparison of numerical predictions to experimental data. More specifically, the effect of the additional source and sink terms, and the modified mathematical expressions for the solid viscosity and granular temperature conduction coefficient are investigated.

The Eulerian-Eulerian TFM proposed by Anderson and Jackson (1967) is used for formulating the governing equations. Additional Fortran subroutines are integrated into the original in-house code in order to implement the new model formulation. The variables predicted include: the mean and fluctuating velocities for both phases, turbulence kinetic

energy, granular temperature, volume fraction, Reynold stresses, eddy viscosity and source terms of the turbulence transport equations.

### 1.4 Organization of the thesis

The present thesis is structured into four chapters as described below.

Chapter 2 presents a broad literature review of multiphase flow. It provides a description and classification of multiphase flow, and outlines the main features of the Eulerian-Eulerian and Eulerian-Lagrangian approaches. It also presents a description of the TFM and KTGF and their constitutive equations. Finally, it gives a summary of the most relevant experimental studies for different cases of liquid-solid flow, including vertical and horizontal flows in pipes and channels.

Chapter 3 describes the methodology of the present thesis. The objective of this chapter is to document the differences between the regular TFM and KTGF model, and a more recent version that considers the effect of the interstitial fluid. Additionally, it presents five different model formulations that are used to assess the effect of different terms in the overall model. Finally, this chapter documents the complete set of equations used in the simulations.

Chapter 4 presents the numerical results. First, predictions are obtained for single phase flow in order to validate the performance of the code. Then, numerical predictions for the five model formulations are compared against the experimental data for one specific mass flow rate. To determine the relevance of the additional and modified terms implemented in the original gas-solid code, different flow variables are analyzed. At the end, the predictions of the best of the five model formulations considered is compared with experimental data for a range of mass flow rates.

Chapter 5 presents the overall of this study and some recommendations for future work.

# Chapter 2: Literature Review

## 2.1 Classification of Flow Regimes

The classification of the flow regime depends on the solids volume fraction $\alpha_s$, which represents the fraction of the volume occupied by the dispersed phase. The volume fraction has a strong influence on many of the hydrodynamic forces, e.g., drag, added mass, etc, as well as the turbulence modulation. The influence of the particle and fluid phases on each other is normally referred to as *coupling*. When the density of the dispersed phase is also considered, the mass loading represents an additional parameter to consider. It relates to the ratio of the mass flux of the dispersed phase to that of the fluid phase, i.e., $m = m_s/m_f$.

Elghobashi (1991; 1994), considers a very dilute regime to exist when $\alpha_s < 10^{-6}$ and the ratio of inter-particle distance to particle diameter is 100 or more $\left(l_{p-p}/d_p \geq 100\right)$. In this regime only one-way coupling exists, i.e. the particle phase is coupled to the fluid phase, but does not affect the fluid phase. When $10^{-6} < \alpha_s \leq 10^{-3}$ and $10 < l_{p-p}/d_p < 100$, the regime is still dilute, but two-way coupling exists, inferring that the velocity field of the fluid phase is modified by the presence of the particles. If the ratio of the particle diameter to the turbulence length scale is lower than 0.1 $\left(d_p/l_T < 0.1\right)$, turbulence is attenuated; if the ratio is greater than 0.1 $\left(d_p/l_T > 0.1\right)$, turbulence is enhanced (Gore and Crowe, 1989). The dense flow regime begins at $\alpha_s \geq 10^{-3}$ and $l_{p-p}/d_p \leq 10$. This regime can be considered as a collision-dominated flow, where a four-way coupling exists. Once the volume fraction becomes sufficiently large ($\alpha_s > 0.1$), contact between particles results in frictional forces, so this regime is considered to be contact-dominated (Crowe *et al*., 1998). The physical behavior of

the contact-dominated flow consists of two sub-categories depending on whether the effect of the fluid can be considered negligible or not (Tsuji, 2000).

## 2.2 Numerical Techniques for Two-Phase Flows

A variety of models exists for the analysis of two-phase flows. However, a successful mathematical formulation that provides accurate predictions and is applicable to a broad range of two-phase flows has not yet been developed. Two of the most popular formulations are given below (Comer, 1998):

1. Two-fluid model (Eulerian-Eulerian)
2. Particle trajectory model (Eulerian-Lagrangian)

The two-fluid model (TFM) presents some advantages over the particle trajectory approach. The TFM considers both phases as interpenetrating continua that interact with each other. It requires less time and computational effort to simulate the system of particles, since it analyzes the system in an Eulerian framework instead of a Lagrangian one. Both phases occupy a fraction of the flow domain, and micro-scale effects are not considered. This advantage becomes more significant as the number of particles increases.

### 2.2.1 Eulerian-Lagrangian approach

The main distinction of this approach is the concept of tracking the path of each particle suspended in a fluid. The local instantaneous differential equations (Messa, 2013) for describing the motion of the fluid phase $f$ and a solid particle $s$ are given by:

Local instantaneous transport equations for the fluid phase:

$$\frac{\partial \rho_f}{\partial t} + \frac{\partial (\rho_f u_i)}{\partial x_i} = 0 \tag{2.1}$$

$$\frac{\partial(\rho_f u_i)}{\partial t} + \frac{\partial(\rho_f u_i u_i)}{\partial x_j} = \frac{\partial \tau_{ij}}{\partial x_j} + \rho_f g_i + \sum_{n=1}^{N_s} F^n(x_i^n)\delta(x - x_i^n) \tag{2.2}$$

Local instantaneous equations of motion for the particles:

$$\frac{\partial x_i}{\partial t} = v_i \tag{2.3}$$

$$m_p \frac{\partial v_i}{\partial t} = F_i \tag{2.4}$$

This method can be attributed to Tsuji *et al*. (1993). In this approach, the fluid flow field is solved within an Eulerian framework. It is determined from the continuity and momentum equations, which can be solved by any appropriate method, e.g. DNS, LES or RANS. On the other hand, the particle trajectories are solved using Newton's equation of motion, i.e., in a Lagrangian framework. Both fields are connected by interphase forces. Unfortunately, the application of the Eulerian-Lagrangian method demands large computational resources, which limits its application for large-scale industrial applications. It is used mostly for dispersed flow conditions.

An extreme application of this method considers particles as point masses with no volume, i.e., the point-particle assumption. This assumption allows the continuity and momentum equations for the fluid to be solved as for single-phase flow. For the case of exceptionally small particles, DNS can be applied for grid sizes smaller than the Kolmogrov scale to solve the instantaneous flow field. Since turbulence is a main factor in determining the particle trajectories, solving the instantaneous fluctuations of the fluid velocity field becomes important. For averaged methods such as LES or RANS, the turbulence is modeled, which becomes a source of uncertainty in Eulerian-Lagrangian solutions (Portella and Oliemans, 2003). Nonetheless, the Eulerian-Lagrangian method is regularly used together with LES or RANS (Armenio *et al*., 1999, Frawley *et al*., 2010, Lain and Sommerfield, 2008).

Some of the most successful implementations of this approach are obtained in combination with the Discrete Element Method (DEM). This method includes inter-particle interaction

forces derived from the concepts of the Hertzian contact stress (Cundall and Strack, 1979, Xiaoliang *et al*., 2018). This method has achieved an impressive development (Zhu *et al*., 2007, Chu *et al*., 2009, Zhou *et al*., 2010), and the most successful applications are related to gas-solid flows and chemical reactions processes (Wu *et al*., 2010, Zhao *et al*., 2010, Zhuang *et al*., 2014). Several commercial software packages (e.g., ANSYS) and open source codes (e.g., OpenFOAM) are capable of applying CFD-DEM in gas-solid flows.

### 2.2.2 Eulerian-Eulerian approach

In this approach, for each control volume, some volume fraction is occupied by the fluid phase $f$ and the remainder by the solid phase $s$, with an interphase that defines the boundary between both phases. The particle phase is modeled as another fluid, so its behavior can be described by similar transport equations. The instantaneous local transport equations (Messa, 2013) applicable to any phase are:

Local instantaneous balance equations for any phase $p$:

$$\frac{\partial \rho_p}{\partial t} + \frac{\partial (\rho_p u_i)}{\partial x_i} = 0 \tag{2.5}$$

$$\frac{\partial (\rho_p u_i)}{\partial t} + \frac{\partial (\rho_p u_i u_i)}{\partial x_j} = \frac{\partial \tau_{pij}}{\partial x_j} + \rho_p g_i \tag{2.6}$$

Equations (2.5) and (2.6) are complemented by another set of equations called the local instantaneous jump conditions, which represent the transfer of mass, energy and momentum across the interface between phases (Messa, 2013, Ishi, 1975, Drew and Passman, 1999). In the Eulerian-Eulerian method, both phases are analyzed in an Eulerian reference frame. The application of any of the various averaging techniques, i.e., time, volume or ensemble, to the local instantaneous equations (2.5) to (2.6) to produce a set of averaged equations results in what is referred to as a two fluid model (TFM). In the averaging process that is performed over the flow domain for both phases, which are treated as continuous and interpenetrating, and the solid phase loses its discrete nature. The averaged mass and momentum conservation equations

for each phase are similar in form. The main advantage of the Eulerian-Eulerian method compared to Eulerian-Lagrangian is that it requires much less computational resources, introduces the volume fraction variable and is able to include the frictional stresses for particle-particle interaction in dense flows cases. However, it does require closure relations to solve the main momentum and turbulence transport equations.

The TFM can also be applied to flows with more than two phases (Ishii, 2006). Some applications for three phases include slurry reactors (Troshko and Zdravistch, 2009), fluidized bed reactors (Panneerselvam *et al*., 2009), biomass analysis (Wang *et al*., 2011) and gas-liquid-solid fluidized beds (Hamidipour *et al*., 2012). The TFM has been used extensively for gas-solid pipe flows and fluidized beds. In addition, the TFM has been widely applied to gas-liquid mixtures, assuming the same bubble size and homogeneous flow (Law *et al*., 2008, Ekambara and Dhotre, 2010), as well as applications to polydisperse flow (Chen *et al*., 2004, Ekambara *et al*., 2008). However, research on liquid-solid applications is still limited, especially for dense flow conditions (Krampa, 2009, Yerrumshetty, 2007).

The modeling of the particles as a continuous phase flow remains a challenge. Different constitutive relations exist to model the particle stress, particle viscosity and particle drag. Some of them consider empirical expressions (Gidaspow, 1994, Enwald *et al*., 1996) and even constant values for the solids viscosity (Sun and Gidaspow, 1999). A better option is the KTGF, which models the solid particles as molecules in a gas to obtain the pseudo-fluid properties, e.g., the solid phase stress, solids viscosity and solids pressure. The properties are dependent on the velocity fluctuations represented by the granular temperature, which is obtained from its own transport equation. The principal reference for this theory is Lun *et al*. (1984), who used the Maxwell transport equation from the kinetic theory of gases to develop a set of constitutive equations to describe the particle phase flow parameters, e.g., granular temperature, particle volume fraction, particle stresses and velocity fluctuations. Louge *et al*. (1991) used the TFM and KTGF in a gas-solid flow to study the influence and interaction between both phases when the fluid flow was turbulent. Bolio *et al*. (1995) modified the KTGF to consider the particle mean free path and added a low-Reynolds number $k-\varepsilon$ model to predict the gas phase

turbulence. Their predicted results were in good agreement with the experimental data of Tsuji *et al*. (1984). In another approach, Cao and Ahmadi (1995), Krampa (2009) and Messa and Stefano (2014) modeled the particle fluctuations in a similar way to the fluid turbulence, considering an eddy viscosity model based on a $k-\varepsilon$ closure for the solid phase. For all approaches, an important aspect is the turbulence modulation effect that particles have on the fluid (e.g. Sinclair and Mallo,1998, Louge *et al*., 1991, Mandø *et al*., 2009).

### 2.2.3 Conservation equations

The TFM conservation equations are generally independent of the averaging process applied to the local instantaneous equations. The Eulerian-Eulerian TFM formulations for the continuity and momentum equations in tensor form are given by (Haghgoo *et al*., 2018):

$$\frac{\partial \alpha_p}{\partial t} + \frac{\partial \left(\alpha_p U_{pi}\right)}{\partial x_i} = 0 \tag{2.7}$$

$$\rho_p \left[\frac{\partial \left(\alpha_p U_{pi}\right)}{\partial t} + U_{pj}\frac{\partial \left(\alpha_p U_{pi}\right)}{\partial x_j}\right] = -\alpha_p \frac{\partial P_f}{\partial x_i} + \frac{\partial \tau_{pij}}{\partial x_j} - \delta \frac{\partial P_s}{\partial x_i} + M_i + \alpha_p \rho_p g_i \tag{2.8}$$

Here, $p$ refers to the fluid ($f$) or particle phase ($s$), respectively; the subscripts *i* and *j* represent the coordinate index used in tensor notation; and the variable $\delta$ is equal to 1 for the solid phase, and otherwise is equal to 0. The variables $\alpha$, $U$, $\beta$, $\rho$, $g$, $P$, $\tau$ represent the volume fraction, mean velocity, interfacial drag coefficient, density, gravity, pressure and stress tensor, respectively.

The first term in the momentum equation (2.8) represents the temporal change, the second is the convective transport, the third is the pressure component due to the fluid phase, the fourth represents an effective stress that includes both the viscous and Reynolds stress components, the fifth is the particle pressure, the sixth is the interfacial momentum transfer and the seventh is the body force due to gravity. The interfacial momentum transfer can include different forces, e.g., Drag, Virtual Mass, Turbulent Dispersion, History, Lift and Brownian motion, each of

which could be important depending on the flow conditions. For example, the virtual mass can be considered negligible for flows with very large density ratios $(\rho_s/\rho_f \gg 1)$, whereas it becomes important for very small density ratios $(\rho_s/\rho_f \ll 1)$. For steady state conditions, the temporal term on the left-hand side of both equations (2.7) and (2.8) disappears. For fully developed flow conditions the convective terms on the left-hand side of Equation (2.8) also vanish.

### 2.3 Additional Concepts

#### 2.3.1 Turbulence

The effective fluid stress tensor $\tau_{fij}$ in equation (2.8) includes the viscous and Reynolds stresses as shown in equation (2.9). For an incompressible fluid phase, the viscous stress follows the model of a Newtonian fluid (equation 2.10), while the Reynolds stress represents correlations of the turbulent velocity fluctuations (equation 2.11). The latter is modeled using an eddy viscosity approach (equation 2.12).

$$\tau_{fij,eff} = \tau_{fij} + R_{ij} = \tau_{fij} - \rho_f \overline{u_i' u_j'} \tag{2.9}$$

$$\tau_{fij} = \mu_{t,f}\left(\frac{\partial U_i}{\partial x_j} - \frac{\partial U_j}{\partial x_i}\right) \tag{2.10}$$

$$-\overline{u_i' u_j'} = \nu_{t,f}\left(\frac{\partial U_i}{\partial x_j} - \frac{\partial U_j}{\partial x_i}\right) - \frac{2}{3}k_f \delta_{ij} \tag{2.11}$$

$$\nu_{t,f} = \frac{C_\mu k_f^2}{\varepsilon_f} \tag{2.12}$$

Here, $\mu_f$ is the viscosity of the fluid, $k_f = \frac{\overline{u_i' u_i'}}{2}$ is the fluid turbulence kinetic energy, $\varepsilon_f = \nu_f \left(\overline{\frac{\partial u_i'}{\partial x_j}\frac{\partial u_i'}{\partial x_j}}\right)$ is its rate of dissipation, $\delta_{ij}$is the Kronecker delta and $\nu_{t,f} = \mu_{t,f}/\rho_f$ is the eddy viscosity. Both variables, $k_f$ and $\varepsilon_f$, are calculated by solving a two-equation $k - \varepsilon$ model,

which for two-phase flow is given by:

$$\frac{\partial(\alpha_f \rho_f k_f)}{\partial t} + \frac{\partial(\alpha_f \rho_f U_j k_f)}{\partial x_j} = \frac{\partial}{\partial x_j}\left[\alpha_f \left(\mu_f + \frac{\mu_{t,f}}{\sigma_k}\right)\frac{\partial k_f}{\partial x_j}\right] + \alpha_f G_{k,f} - \alpha_f \rho_f \varepsilon_f + S_{k,f} \qquad (2.13)$$

$$\frac{\partial(\alpha_f \rho_f \varepsilon_f)}{\partial t} + \frac{\partial(\alpha_f \rho_f U_j \varepsilon_f)}{\partial x_j} = \frac{\partial}{\partial x_j}\left[\alpha_f \left(\mu_f + \frac{\mu_{t,f}}{\sigma_\varepsilon}\right)\frac{\partial \varepsilon_f}{\partial x_j}\right] + \alpha_f \frac{\varepsilon_f}{k_f}\left(C_{\varepsilon 1} G_{k,f} - C_{\varepsilon 2} \rho_f \varepsilon_f\right) + S_{\varepsilon,f} \qquad (2.14)$$

where $G_{k,f} = -\overline{u_i' u_j'}\frac{\partial U_i}{\partial x_j}$ is the production of turbulence kinetic energy. The source terms, $S_{k,f}$ and $S_{\varepsilon,f}$, represent the influence of the particle phase on the fluid turbulence, i.e. the turbulence modulation.

**Table 2.1:** Numerical constants of $k-\varepsilon$ model (Crowe *et al.*, 2012).

| $\sigma_k$ | $\sigma_\varepsilon$ | $C_{\varepsilon 1}$ | $C_{\varepsilon 2}$ | $C_{\varepsilon 3}$ | $C_\mu$ |
|---|---|---|---|---|---|
| 1.00 | 1.30 | 1.44 | 1.92 | 1.00 | 0.09 |

Turbulence changes significantly in the near-wall region, and reduces to zero at the wall. In order to reproduce this behavior, a variety of damping functions have been implemented in equations (2.13) and (2.14), resulting in so-called low Reynolds number formulations. Hrenya *et al*. (1995) performed a study of ten models and concluded that the LRN model of Myong and Kasagi (1990) performed the best. An alternate approach is the so-called two-layer model of Chen and Patel (1988), which was later modified by Durbin *et al*. (2001) to include the effects of the surface roughness.

### 2.3.2 Turbulence Modulation

Turbulence modulation relates to the coupling of the fluctuating velocity fields of both phases. The fluid and solid phases are connected through a generalized interfacial drag term that

couples the mean velocities of both phases. When only the drag force is considered, the selection of the appropriate expression for the drag coefficient $C_D$ becomes relevant. Following Mandø *et al*. (2009), turbulence modulation models can be classified as given in Table 2.2.

The standard and consistent models are able to predict only turbulence attenuation and enhancement, respectively. On the other hand, the new model proposed by Mandø *et al*. (2009) is able to predict both effects. In the equations above, $|U_i - V_i|$ is the modulus of the relative mean velocity, $\overline{u_i' v_i'}$ represents the correlation between the fluctuating velocity fields of the fluid and solid phases, $\overline{v_i' v_i'}$ represents the turbulence fluctuations in the solids velocity field and $\tau_p$ is the particle response timescale. Crowe *et al*. (2012) performed volume averaging and in the consistent model obtained similar terms, i.e., the term $|U_i - V_i|^2$ refers to the generation of $k_f$ due to particle drag and the term $\overline{v_i' v_i'} - \overline{u_i' v_i'}$ is the redistribution of $k_f$.

**Table 2.2:** Turbulence modulation models based on drag force.

| **Approach** | $S_{k,f}$ | **Prediction capability** |
|---|---|---|
| Standard | $\alpha_s \rho_s \left(\overline{u_i' v_i'} - 2k_f\right)/\tau_p$ | Attenuation |
| Consistent | $\alpha_s \rho_s \left(\lvert U_i - V_i \rvert^2 + \overline{v_i' v_i'} - \overline{u_i' v_i'}\right)/\tau_p$ | Enhancement |
| New model | $\alpha_s \rho_s \left(\lvert U_i - V_i \rvert^2 + \overline{v_i' v_i'} - 2k\right)/\tau_p$ | Both |

### 2.3.3 Kinetic Theory of Granular Flow (KTGF)

Based on equation (2.8) the momentum transport equation for the solid phase can be expressed as follows:

$$\frac{\partial(\alpha_s \rho_s V_i)}{\partial t} + \frac{\partial(\alpha_s \rho_s V_i V_i)}{\partial x_j} = -\alpha_s \frac{\partial}{\partial x_i} P_f - \frac{\partial}{\partial x_i} P_s + \frac{\partial}{\partial x_j}\left(\alpha_s \tau_{sij}\right) + \alpha_s \rho_s g_i + M_i \qquad (2.15)$$

Here, the first term on the right hand side of equation (2.15) represents the buoyancy force of the particle. In the next term, $P_s$ is the particle pressure that is extracted from the particle stress,

and $\tau_{sij}$ is function of the solid viscosity $\mu_s$. To calculate these properties, one can model the particle flow as that of a pseudo-fluid. The KTGF is an analogy to the kinetic theory of gases in thermodynamics, but applied to a dispersed field of particles. The KTGF yields constitutive relations for the particle stresses, as well as the relevant particle properties such as $\mu_s$. Both $P_s$ and $\mu_s$ can be decomposed in two main contributions, i.e., equations (2.16) and (2.17). The first contribution is the kinetic component that applies when particles travel freely between collision periods, and the second is the collisional component that derives from collision between particles.

$$P_s = P_{s,Kin} + P_{s,coll} \tag{2.16}$$

$$\mu_s = \mu_{s,Kin} + \mu_{s,coll} \tag{2.17}$$

The particle velocity fluctuations, represented by the granular temperature $T$, can be obtained by solving its respective transport equation (2.18), given by:

$$\frac{3\alpha_s\rho_s}{2}\left[\frac{\partial T}{\partial t} + \frac{\partial\left(V_j T\right)}{\partial x_j}\right] = \frac{\partial}{\partial x_j}\left(\kappa_s \frac{\partial T}{\partial x_j}\right) - P_s\frac{\partial V_i}{\partial x_i} + \tau_{ij}\frac{\partial V_i}{\partial x_j} - \frac{\alpha_s\rho_s}{\tau_p}(3T - \overline{u_i' v_i'}) - \gamma_s \tag{2.18}$$

Here $T = \overline{v_i' v_i'}/3$ is the granular temperature, $\kappa_s$ is the granular conductivity, $3T$ is the dissipation rate resulting from the drag force (viscous damping), $\overline{u_i' v_i'}$ term is the production due to interaction between fluctuation fields and $\gamma_s$ is the dissipation due to particle collisions.

Constitutive equations for the solids viscosity $\mu_s$, solids pressure $P_s$ and their respective dependence on the granular temperature have been proposed by several authors for a wide range of applications (Lun *et al*., 1984, Gidaspow, 1994, Sinclair and Jackson, 1989, Johnson *et al*., 1990, Schaeffer, 1987, Lun and Savage, 1986, Srivastava and Sundaresan, 2003, Ocone *et al*., 1993). Some of these are considered further in Chapter 3 of the present thesis.

## 2.4 Previous experimental studies

Since liquid-solid flow in vertical pipes is not often encountered in industry, it has not been studied as extensively as flow in horizontal pipes. For slurry flows, the work of Sumner (1992) remains one of the most cited for vertical pipes. He used five types of particles, i.e, gravel, medium sand, coarse sand, fine plastic and coarse plastic, and obtained measurements for the particle velocity and concentration profiles for bulk solids concentrations ranging from 10% to 50% in pipes of diameter 25.8 and 40 mm. Krampa (2009) performed experiments using glass beads of diameter 0.5 mm and 2 mm in a 53 mm pipe for bulk solids concentration up to 45%. He collected data on the local solids velocity and pressure drop. For dispersed flow, Alajbegovic *et al*. (1994) worked with bulk solids concentrations ranging from 1% to 4%. He used ceramic and polystyrene particles in a vertical pipe of diameter 30.6 mm. For horizontal applications, Gillies (1993) performed measurements of the pressure drop, as well as the solids concentration and velocity profiles for coarse-particle slurry flows using sand and coal up to a volume fraction of 35%. A broad summary of some of the most significant experimental work is presented in Table 2.3 and 2.4.

**Table 2.3:** Experimental studies for liquid-solid flow in channels.

| **Channel** | **Flow direction** | $\rho_p / \rho_f$ | $\alpha_s$ | $d_p$ **(mm)** | ***Re*** |
|---|---|---|---|---|---|
| Suzuki *et al.* (1999) | Vertical Down | 3850 | $3.2\times10^{-4}$ | 0.4 | 7200 |
| Kiger and Pan (2002) | Horizontal | 2.5 | $2.4\times10^{-4}$ | 0.195 | 25000 |
| Sato *et al.* (1995) | Vertical Down | 2.5 | 0.002 - 0.013 | 0.34, 0.5 | 5000 |

**Table 2.4:** Experimental studies for liquid-solid flow in pipes.

| Pipe | Flow direction | $\rho_p / \rho_f$ | $\alpha_s$ | $d_p$ (mm) | Re | $U$(m/s) | Pipe D(m) |
|---|---|---|---|---|---|---|---|
| Gillies (1993) | Horizontal | 2.65 | 0.19 - 0.33 | 0.09-0.27 | 103,000 – 515,000 | 1.0 - 5.0 | 0.103 |
| Korving (2002) | Horizontal | 2.65 | 0.18 - 0.48 | 0.1 | 237,000 – 632,000 | 1.5 - 4.0 | 0.158 |
| Schaan (2001) | Horizontal | 2.44 - 2.65 | 0.139 - 0.40 | 0.085-0.09 | 62,500 - 800,000 | 1.25 - 5.0 | 0.05 - 0.16 |
| Sumner (1992) | Vertical Up | 1.05 - 2.65 | 0.1 - 0.5 | 0.29-1.7 | 50,000 - 280,000 | 2.0 - 7.0 | 0.025 - 0.04 |
| Krampa (2009) | Vertical Up | 2.5 | < 0.45 | 0.5 - 2.0 | 53,000 - 265,000 | 1.0 - 5.0 | 0.053 |
| Hashemi *et al.* (2014) | Horizontal | | 0.2 - 0.35 | 0.1 | 104,000 – 260,000 | 2.0 - 5.0 | 0.052 |
| Kameyama *et al.* (2014) | Up/down | 2.5 | 0.006 | 0.625 | 19,500 | 0.75 | 0.026 |
| Hosokawa and Tomiyama (2004) | Vertical Up | 3.2 | 0.007 - 0.018 | 1 to 4 | 15,000 | 0.5 | 0.03 |
| Alajbegovic *et al.* (1994) | Vertical Up | 0.032, 2.45 | 0.009 - 0.036 | 1.79, 2.32 | 42,000 - 68,000 | 1.3 - 2.2 | 0.0306 |
| Zisselmar and Molerus (1979) | Horizontal | 2.5 | 0.017 - 0.056 | 0.053 | 100,000 | 2.0 | 0.05 |

## 2.5 Previous in-house numerical research

Several research studies that consider simulation of two-phase flow, using either commercial software or in-house codes, have been performed at the University of Saskatchewan by the CFD group headed by Prof D. J. Bergstrom. For example, Krampa-Morlu *et al*. (2004) used ANSYS to compare numerical results to the experimental data of Sumner *et al*. (1990) and obtained good agreement for the mean solids velocity profile; however, the solids concentration prediction gave mixed results. In a later work, Krampa-Morlu (2009) used the commercial software ANSYS CFX to analyze three closure models (i.e., $k_f - \varepsilon_f - k_s - \varepsilon_s, k_f - \varepsilon_f - k_s - \varepsilon_s - T_s, k_f - \varepsilon_f - k_s - k_{fs}$). He compared the predicted results with the experimental data of Sumner *et al*. (1990), and obtained good predictions for the mean solids velocity and concentration profiles for all three models for concentrations below 10%, but was less successful for higher concentrations. More recently, Haghgoo *et al*. (2018) used the Multiphase Flow with Interphase eXchanges (MFIX) software to perform numerical simulations of bubbling fluidized beds.

Yerrumshetty (2007) used an in-house code based on the two-fluid model of Bolio *et al*. (1995) and the LRN $k - \varepsilon$ model of Myong and Kasagi (1990) to predict both gas-solid and liquid-solid flows. For the gas-solid case, results were compared to the data of Tsuji *et al*. (1984) obtaining good agreement with the mean velocity profile for both phases, i.e., gas and solid. For the liquid-solid case, predictions for the flows of Alajbegovic *et al*. (1994) and Summer *et al*. (1990) showed mixed results, especially for the volume fraction profile. Zaman and Bergstrom (2012) modified the in-house code used by Yerrumshety (2007) to perform simulations of gas-solid flows in vertical pipes. They compared the performance of some turbulence modulations models, i.e., Rao *et al*. (2012) and Crowe (2000), obtaining good predictions for the mean velocity profile for both phases, but unrealistic predictions for the granular temperature. A complementary work was performed to analyze the performance of the two-layer model in rough pipes. The theory of granular temperature was used to describe the solid-phase velocity fluctuation and the $k - \varepsilon$ model for the gas-phase turbulence. Das (2017) worked with the same in-house code reconfigured to simulate gas-solid flow in horizontal

channel. He used the two-layer model of Durbin *et al*. (2001) to analyze the effect of wall roughness on the particle transport. His simulation adopted the two fluid model formulation of Rao *et al*. (2012) and made comparison to the experimental work of Sommerfeld and Kussin (2004).

# Chapter 3: Methodology

## 3.1 Introduction

The present chapter focuses on the study of the TFM for the specific case of a fully developed turbulent liquid-solid flow in a vertical pipe. In this chapter, specific equations in radial coordinates are derived from the ones presented in Chapter 2. The main intention is to evaluate and compare the TFM formulations for gas-solid flow with respect to a recent version used for liquid-solid flow, which considers the interstitial fluid effect. In this context, both formulations are presented and discussed to highlight the difference between them, and three intermediate formulations are included with the main purpose of evaluating the effect of the extra terms in the predicted results when compared to the experimental data. The evaluation includes variables such as mean velocity, solids volume fraction, turbulence kinetic energy, Reynolds shear stress, and a profound study of the source terms of the turbulence kinetic energy and granular temperature transport equations. Finally, the best formulation is compared with experimental data for different mass flow rates. As a preliminary step, before the multiphase flow results, a single-phase flow evaluation is performed with the intention to validate the performance of the in-house code.

The TFM has been shown to perform well for gas-solid flows and fluidized beds, but is still deficient for liquid-solid flow. The main difficulties relate to modeling the additional physics that become relevant in liquid-solid flow, i.e., the interstitial fluid effect. To include this effect requires additional source terms in the transport equations for the turbulence kinetic energy and granular temperature. In the literature, Peirano and Leckner (1998) highlight the relevance of

the interstitial fluid in the granular flow model

Solid particles suspended in a fluid can enhance or diminish the intensity of the turbulence depending on the solids volume fraction $\alpha_s$. Note that, both conditions can occur in the same flow, i.e., particle contact in regions of high concentration reduces the turbulence, while in low concentration regions the generation of wakes enhances turbulence. In general, flows with a high mass loading display an attenuation of turbulence. In addition, following Crowe (2000), if the ratio of the particle diameter to the turbulence length scale is smaller than 0.1, turbulence is attenuated, while for a ratio higher than 0.1, turbulence is enhanced. This description indicates that small particles tend to diminish turbulence, while larger particles tend to enhance it due to the generation of particle wakes.

An important parameter to measure particle behavior is the particle response timescale $(\tau_P)$, which represents the time for a particle to achieve 65% of the fluid field velocity starting from rest. A related parameter is the Stokes number $(S_T)$, which is the ratio of the particle response timescale to the timescale of the flow field $(\tau_f)$. For example, for a pipe flow, the value of $\tau_f$ is often taken as the pipe diameter divided by the bulk fluid velocity. For this case, Stokes number can be referred to as the domain Stokes number (Loth, 2011), i.e., $S_T = \tau_P/\tau_f$. If $S_T \gg 1$, the particle responds very slowly to a change in the macroscopic flow field, so that the turbulence field only weakly affects the particle motions. Whereas, for $S_T \approx 1$ the macroscopic fluid flow substantially affects the particle motion. Similar arguments can be applied when considering the influence on the particle motion of the time scales of the turbulence, i.e., the smallest scales such as the Kolmogorov scale are characterized by the micro-scale Stokes number. As noted previously, the effect of particles on the fluid turbulence is usually referred to as Turbulence Modulation, and is often modeled by an additional source terms in the turbulence transport equations typically used with the TFM. Popular turbulence modulation models are those of Crowe (2000), Louge *et al*. (1991) and Rao *et al*. (2012); the latter includes an explicit term for the wake generation.

To simulate the physical properties of the solid phase, the KTGF has been successful in

applications to gas-solid flows (Lun *et al*., 1984, Jenkins and Savage, 1983) and fluidized beds (Ding and Gidaspow, 1990, Lun *et al*., 1984). The KTGF uses the Maxwell transport equation to develop a set of equations to calculate the properties of particle phase, e.g., granular temperature, particle pressure, volume fraction, velocity fluctuation and solid phase stress. Louge *et al*. (1991) incorporated the KTGF into a TFM to study the influence of the fluctuating velocity field of one phase on the other for gas-solid flow in a pipe. Bolio *et al*. (1995) expanded this work and used a LRN $k-\varepsilon$ model to simulate the gas phase turbulence. The predictions of Bolio *et al*. (1995) showed good agreement with the experimental data of Tsuji *et al*. (1984). Hadinoto and Curtis (2004) noted that Jones and Sinclair observed that the predicted velocity fluctuations of particles were larger than the experimental values, i.e., there was some energy that going somewhere else. In this case, it was inferred that the interstitial fluid dissipates part of the solids fluctuating energy (granular temperature). The reason behind this erroneous model performance can be attributed to the fact that model of Lun *et al*. (1984) neglected the effect of the interstitial fluid, i.e., the equations were derived considering vacuum conditions. Hadinoto and Curtis (2004) investigated how the particle-particle collisions are influenced by the interstitial fluid in dispersed liquid-solid and gas-solid flow with reference to the previous works of Lun and Savage (1987) and Lun and Savage (2003). Hadinoto and Curtis (2004) used the KTGF for predicting the solid phase properties, but included some modifications in the calculation of the solids viscosity and the diffusion coefficient of the granular temperature. In addition, they introduced two different particle coefficients of restitution to evaluate the fraction of kinetic energy dissipated by the inelasticity of the particle-particle collisions, one in a vacuum $(e_s)$ and the other when an interstitial fluid exists $(e_f)$. Here, $e_f$ includes the viscous effect of the fluid on the collision of the particle surfaces, which was documented in the experimental research of Gondret *et al*. (2002). In a more recent study, Hadinoto (2010) expanded his previous work to analyze the prediction of turbulence modulation by comparing the turbulence closure expressions of Louge *et al*. (1991) and Sinclair and Mallo (1998) at different Reynolds numbers, which resulted in some additional modifications in the turbulence kinetic energy transport equations.

As mentioned, most of the research in two-phase flow of particles in a fluid has been developed for gas-solid flow (e.g. Bolio *et al*., 1995, Peirano and Leckner, 1998, Sinclair and

Jackson, 1989, Kenning and Crowe, 1997, and Zhang and Reese, 2001, Zhang and Reese, 2003, Zaman and Bergstrom, 2014). In contrast, only a few references are found in the literature for liquid-solid flow (e.g. Krampa-Morlu *et al*., 2004, Hadinoto and Curtis, 2004, and Hadinoto, 2010). For gas-solid flow the interstitial fluid effect can be neglected, but for liquid-solid flow this contribution is significant. In this context, the present research work is intended to compare the formulations of Bolio *et al*. (1995), Hadinoto and Curtis (2004) and Hadinoto (2010), and apply them to the same experimental case of dispersed liquid-solid flow in a vertical pipe.

The numerical predictions are compared to the experimental data of Alajbegovic *et al*. (1994), who studied dispersed liquid-solid flow (upward direction) in a vertical pipe of 30.6 mm diameter with bulk volume fractions from 1% to 4%. The carrier phase was water and the dispersed phase was ceramic particles ($d_p$= 2.32 mm, $\rho_f$= 2443 kg/m$^3$). Their paper presents substantial information on the experimental conditions, which is essential for replication using numerical simulations. In addition, this work is readily handled by the in-house numerical code since it considers fully developed flow. The extensive experimental data set includes measurements of the solid volume fraction, and both mean and fluctuating velocities of both phases.

### 3.2 Models Description

A detailed description and discussion of the models of Bolio *et al*. (1995) for gas-solid flow and Hadinoto and Curtis (2004) for liquid-solid flow is presented below. These two base models and three additional models are studied. The three additional models each include parts of the base models, and are used to analyze the effect and relevance of the additional terms intended to incorporate the effects of the interstitial fluid for a liquid-solid flow. Of special interest is the effect of the modeling on the profiles of the granular temperature and volume fraction profile in the near-wall region. In addition, the behavior of the different terms in the transport equations for the turbulence kinetic energy and granular temperature is analyzed to elucidate their relevance and contribution in the numerical predictions. The present section develops the general equations presented in Chapter 2 for the specific case of fully developed upward vertical

flow in a pipe using the model formulations given above.

### 3.2.1 Momentum Transport Equations

The TFM of Bolio *et al*. (1995) and Hadinoto and Curtis (2004) in radial coordinates and simplified for the case of fully developed flow can be summarized as follows:

Fluid momentum balance:

$$0 = \frac{1}{r}\frac{\partial}{\partial r}\left[\alpha_f r \tau_{rz}^f\right] - \alpha_f \frac{\partial P_f}{\partial z} - \beta(U - V) + \alpha_f \rho_f g + G_{inter} \tag{3.1}$$

Fluid shear stress

$$\tau_{rz}^f = \mu_{ef}\frac{\partial U}{\partial r} - \rho_f \overline{u_z' u_r'} = \left(\mu_{ef} + \mu_t\right)\frac{\partial U}{\partial r} \tag{3.2}$$

Particle momentum balance:

$$0 = \frac{-1}{r}\frac{\partial}{\partial r}(r\tau_{rz}^s) - \alpha_s \frac{\partial P_f}{\partial z} + \beta(U - V) + \alpha_s \rho_s g \tag{3.3}$$

$$0 = \frac{1}{r}\frac{\partial}{\partial r}(r\sigma_{rr}) - \frac{\sigma_{\theta\theta}}{r} \tag{3.4}$$

Solids shear stress:

$$\tau_{rz}^s = -\mu_S^*(\omega G_{1k} + G_{1c})\frac{\partial V}{\partial r} \tag{3.5}$$

Solids normal stresses:

$$\sigma_{rr}^s = \rho_s(\omega G_{2k} - G_{2c})T \tag{3.6}$$

Here, $\tau_{rz}^f$ is the total shear stress of the fluid, $\overline{u_z' u_r'}$ is the Reynolds shear stress and is modeled using the eddy viscosity approach where $\mu_t = C_\mu f_\mu \rho_\mu k^2/\varepsilon$ , and $\mu_{ef}$ is the effective fluid viscosity, which includes the effect of the particles in the fluid.. The subscripts $k$ and $c$ in equations (3.5) and (3.6) indicate the kinetic and collisional contributions, respectively, and $\sigma_{rr}$ and $\sigma_{\theta\theta}$ are the normal stresses in the radial and azimuthal direction, respectively.

For Bolio *et al*. (1995) the effective viscosity is the same as the molecular viscosity, i.e., $\mu_{ef} = \mu_f$, whereas for Hadinoto and Curtis (2004) is calculated using equation (3.7):

$$\mu_{ef} = \mu_f(1 - \alpha_s - 0.33\alpha_s^2)^{-2.5} \tag{3.7}$$

Equation (3.7) indicates that the higher the solids volume fraction, the larger the effective viscosity.

**Table 3.1:** Constitutive equations for particle stress.

| $\boldsymbol{\tau_{rz}^s}$ | $\boldsymbol{\sigma_{rr}^s}$ |
|---|---|
| $G_{1k} = \frac{1}{\eta(2-\eta)g_o}\left[1 + \frac{8}{5}\eta\alpha_s g_o(3\eta - 2)\right]$ | $G_{2k} = \alpha_s$ |
| $G_{1c} = \frac{8\alpha_s}{5(2-\eta)}\left[1 + \frac{8}{5}\eta\alpha_s g_o(3\eta - 2)\right] + \frac{768\alpha_s^2 g_o \eta}{25\pi}$ | $G_{2c} = 4\eta\alpha_s^2 g_o$ |

The work of Hadinoto and Curtis (2004) includes a new source term in the fluid momentum equation (3.1) to account for the effects of particle collisions, i.e., $G_{inter} = \frac{\eta_s - \eta_f}{\eta_f}\frac{1}{r}\frac{\partial}{\partial r}\left(r\mu_S^* G_{1c}\frac{\partial u_s}{\partial r}\right)$, where the parameter $\eta$ is calculated as a function of $e_f$, i.e., $\eta = \frac{1+e_f}{2}$. The $G_{inter}$ term is based on the previous work of Lun and Savage (1987) and Lun and Savage (2003), which included the contribution of the particle collision as a new source term in the fluid momentum equation. The rationale is that when particles move in a vacuum, some energy is dissipated by particle-particle collisions, which is represented by the coefficient of restitution $e_s$. However, to account for the presence of a real fluid, it is necessary to consider that particles lose energy during collisions by displacing the fluid; thus, particles lose additional energy as they do work on the fluid, which is accounted for by a new coefficient of restitution $e_f < e_s$. Note that Bolio *et al*. (1995) assumed $G_{inter} = 0$ and $\eta = \frac{1+e_s}{2}$. The constitutive expressions to calculate the solid viscosity $\mu_S^*$ and the drag coefficient $\beta$ for each model are presented in Table 3.2 and Table 3.3, respectively.

**Table 3.2:** Constitutive expressions for the solids viscosity $\mu_S^*$ for both models.

| **Bolio *et al.* (1995)** |
|---|
| $$\mu_S^* = \mu_s = \frac{5\sqrt{\pi} d_P \rho_s \sqrt{T}}{96}$$ |
| $$\omega = \frac{1}{1-\lambda/R} \qquad \lambda = \frac{d_P}{6\sqrt{2}\alpha_s} \qquad g_o = \frac{\alpha_o^{1/3}}{\alpha_o^{1/3} - \alpha_s^{1/3}}$$ |
| **Hadinoto and Curtis (2004)** |
| $$\mu_S^* = \frac{\mu_1^*}{\mu_1}\mu_s \qquad \mu_s = \frac{5\sqrt{\pi} d_P \rho_s \sqrt{T}}{96} \qquad \mu_1 = \frac{\mu_s}{\eta_f(2-\eta_f)} \qquad \mu_1^* = \frac{\mu_1}{1 + \frac{2\xi_d \mu_1}{c_s \rho_S g_o T}}$$ |
| $$\omega = \frac{1}{1-\lambda/R} \qquad \lambda = \frac{d_P}{6\sqrt{2}\alpha_s} \qquad \xi_d = \frac{3}{4}\frac{\rho_f}{\rho_s}\frac{C_D}{d_p}\left\|u_f - u_s\right\| \qquad g_o = \frac{\alpha_o^{1/3}}{\alpha_o^{1/3} - \alpha_s^{1/3}}$$ |

Here, $\mu_S$ represents the particle shear stress in a vacuum, $\mu_S^*$ is the modified expression for the particle viscosity when an interstitial fluid is present, $\xi_d$ is the specific friction coefficient of the fluid, $g_o$ is the radial distribution function, $\omega$ is a damping function, $\lambda$ is the mean free path and $T = \overline{v_i' v_i'}/3$ is the granular temperature.

**Table 3.3:** Constitutive expressions for the drag coefficient $\beta$ for both models.

| **Bolio *et al.* (1995)** | **Hadinoto and Curtis (2004)** |
|---|---|
| $\beta = \frac{3\rho_f C_D \alpha_s \lvert U - V \rvert}{4 d_P (1-\alpha_s)^{2.65}}$ | $\beta = \frac{3\rho_f C_D \alpha_s \lvert U - V \rvert}{4 d_P (1-\alpha_s)^{2.65}}$ |
| $C_D = \frac{24}{R_p}\left(1 + 0.15 R_p^{0.687}\right)$ | $C_D = \left(\frac{24}{R_p} + \frac{4}{R_p^{1/2}} + 0.4\right)(1 - \alpha_s - 0.33\alpha_s^2)^{-2.5}$ |
| $R_p = (1-\alpha_s)\frac{\rho_f d_p \lvert U - V \rvert}{\mu_f}$ | $R_p = \frac{\rho_f d_p \lvert U - V \rvert}{\mu_f}$ |

Here, $d_p$ is the particle diameter, $C_D$ is the drag coefficient and $R_p$ is the particle Reynolds number. Note that the interfacial drag coefficient $\beta$ does not consider the fluid volume fraction as defined in the original expression proposed by Wen and Yu (1966). A possible reason may

be that the flows studied by Bolio *et al*. (1995) only considered the dilute flow regime, for which $\alpha_f = 1 - \alpha_s \approx 1$. The same consideration may apply to the $R_p$ used by Hadinoto and Curtis (2004). For the drag coefficient $C_D$, Bolio *et al*. (1995) used the expression of Wen and Yu (1966), whereas Hadinoto and Curtis used the expression of Lun and Savage (1987).

### 3.2.2 Turbulence Equations

To account for turbulence, the eddy viscosity $\mu_t = C_\mu f_\mu \rho_\mu \, k^2/\varepsilon$ and the LRN $k-\varepsilon$ turbulence model of Myong and Kasagi (1990) are used for calculation of the turbulence kinetic energy $k$ and dissipation rate $\varepsilon$. The transport equations in radial coordinates and simplified for fully developed flow are given by:

Turbulence kinetic energy:

$$0 = \frac{1}{r}\frac{\partial}{\partial r}\left[r(1-\alpha_s)\left(\mu_{ef} + \frac{\mu_t}{\sigma_k}\right)\frac{\partial k}{\partial r}\right] + (1-\alpha_s)\mu_t\left(\frac{\partial U}{\partial r}\right)^2 - \rho_f(1-\alpha_s)\varepsilon + I_k + S_{k,IT} \quad (3.8)$$

Dissipation rate:

$$0 = \frac{1}{r}\frac{\partial}{\partial r}\left[r(1-\alpha_s)\left(\mu_{ef} + \frac{\mu_t}{\sigma_\varepsilon}\right)\frac{\partial \varepsilon}{\partial r}\right] + c_{\varepsilon 1} f_1 \frac{\varepsilon}{k}(1-\alpha_s)\mu_t\left(\frac{\partial U}{\partial r}\right)^2 - c_{\varepsilon 2} f_2 \rho_f (1-\alpha_s)\frac{\varepsilon^2}{k} + c_{\varepsilon 3} f_2 I_k \frac{\varepsilon}{k} + S_{\varepsilon,IT} \quad (3.9)$$

**Table 3.4:** Damping functions and constants for the LRN model of Myong and Kasagi (1990).

$$f_1 = 1.0, \quad f_2 = 1 - (2/9)exp\{-(R_t/6)^2\}, \quad f_\mu = 1 + 3.45/\sqrt{R_t}$$

$$y^+ = \frac{(R-r)u_\tau}{\nu_f} \quad , \quad R_t = \frac{k^2}{\nu_f \varepsilon}$$

| $\sigma_k$ | $\sigma_\varepsilon$ | $C_{\varepsilon 1}$ | $C_{\varepsilon 2}$ | $C_{\varepsilon 3}$ | $C_\mu$ |
|---|---|---|---|---|---|
| 1.4 | 1.3 | 1.4 | 1.8 | 1.2 | 0.09 |

The first four terms in Equation (3.8) represent the diffusion, production, dissipation and turbulence modulation, respectively, and $S_{k,IT}$ is an additional source term due to the interstitial fluid effects as proposed by Hadinoto and Curtis (2004). In addition, $y^+$ is the wall-normal distance in wall units, $u_\tau$ is the wall velocity, $\nu_f$ is the fluid kinematic viscosity and $R_t$ is the turbulence Reynolds number. Similarly, the expression for the turbulence modulation $I_k$ and the turbulence closure to model the correlation between the fluid and solids fluctuating velocity fields $\overline{u_i' v_i'}$ are given by Sinclair and Mallo (1998) as follows:

$$I_k = \beta(\overline{u_i' v_i'} - 2k) \tag{3.10}$$

$$\overline{u_i' v_i'} = \sqrt{2k}\sqrt{3T} \tag{3.11}$$

With respect to the interstitial fluid source term $S_{k,IT}$, Bolio *et al*. (1995) assumed $S_{k,IT} = S_{\varepsilon,IT} = 0$, whereas Hadinoto and Curtis (2004) proposed the models given in Table 3.5.

**Table 3.5:** Additional source terms for the turbulence kinetic energy and dissipation rate transport equations when the effect of the interstitial fluid is included.

| **Hadinoto and Curtis (2004)** |
|---|
| $S_{k,IT} = E_W + \frac{\eta_s - \eta_f}{\eta_f}\mu_S^* G_{1c}\frac{\partial V}{\partial r}\frac{\partial U}{\partial r} + \gamma_{FKET} - S_{p-p}$ |
| $S_{\varepsilon,IT} = c_{\varepsilon 3} f_2 \frac{\varepsilon}{k} E_W + c_{\varepsilon 1} f_1 \frac{\varepsilon}{k}\frac{\eta_s - \eta_f}{\eta_f}\mu_S^* G_{1c}\frac{\partial V}{\partial r}\frac{\partial U}{\partial r} + c_{\varepsilon 1} f_1 \frac{\varepsilon}{k}\gamma_{FKET} - c_{\varepsilon 3} f_2 \frac{\varepsilon}{k} S_{p-p}$ |
| $E_W = 2\pi C_W n d_p \rho_f \nu_t k \qquad \nu_t = \nu_f 0.017 R_p \qquad C_W = 16/3$ |
| $\gamma_{FKET} = (1-\bar{\beta})\gamma \qquad \bar{\beta} = \frac{1-e_s^2}{1-e_f^2}$ |
| $S_{p-p} = 3\varphi\beta T \qquad \varphi = 1 + 0.88\alpha_s$ |

The first term of $S_{k,IT}$ is the energy generated by particle wakes $E_W$, the second is the generation due the collisional fluid stress, the third is a source of fluid turbulence kinetic energy due to particle collisions, $\gamma_{FKET}$, and the fourth is a sink term due to the long range effects of particle interactions within the fluid phase, $S_{p-p}$. In the model relations, $n$ is the particle number

density, $\gamma$ is the dissipation of granular temperature, $\varphi$ is the absorption coefficient of the turbulence kinetic energy and $\bar{\beta}$ is a ratio of the particle fluctuating energy lost by heat due to particle-particle inelastic collisions relative to the total energy lost by heat and fluid interactions.

### 3.2.3 Granular Temperature

The granular temperature $T$ represents the averaged fluctuating kinetic energy of the particles, in a similar way as the thermodynamic temperature represents an average of the kinetic energy of the molecules in a gas. Transport equation (3.12) is used to calculate the distribution of the granular temperature. The first term represents conduction (also referred to as diffusion), the second term is the production of $T$ due to the particle shear stress and velocity gradients, the third term is the dissipation due to inelastic particle-particle collisions (Sinclair & Jackson, 1989), the fourth term is the turbulence modulation and the last term is a contribution due long-range interaction between particles via the fluid.

$$0 = \frac{-1}{r}\frac{\partial}{\partial r}(rq_{PT}) - \tau_{rz}^{s}\frac{\partial V}{\partial r} - \gamma + I_T + S_{p-p} \tag{3.12}$$

$$q_{PT} = -\lambda^{*}(\omega G_{3K} + G_{3c})\frac{\partial T}{\partial r} \tag{3.13}$$

$$\gamma = \frac{48}{\sqrt{\pi}}\eta_f(1-\eta_f)g_o\alpha_o^2\frac{\rho_s}{d_P}T^{\frac{3}{2}} \tag{3.14}$$

In the transport equation for $T$, $q_{PT}$ is the flux of pseudo-thermal energy and $\gamma$ is the dissipation rate of the granular temperature. If particle-particle collisions are perfectly elastic ($e_s = 1$), then $\gamma \to 0$ and the energy dissipation is zero. The turbulence modulation term is given by $I_T = \beta(\overline{u_l' v_l'} - 3T)$. For Bolio *et al*. (1995) who considered particles in a gas, $S_{p-p} = 0$, whereas for Hadinoto and Curtis (2004) who considered particles in a liquid, $S_{p-p} = -3\alpha\beta T$. The constitutive equations developed by Lun *et al*. (1984), with a few variations from Hadinoto and Curtis (2004), are given by equations (3.13), (3.14) and the model relations in Table 3.6 and 3.7.

**Table 3.6:** Constitutive equations for granular temperature.

| $\boldsymbol{q_{PT}}$ |
|---|
| $G_{3k} = \frac{8}{\eta_f(41-33\eta_f)g_o}\left[1+\frac{12}{5}{\eta_f}^2\alpha_s g_o(4\eta_f-3)\right]$ |
| $G_{3c} = \frac{96\alpha_s}{5(41-33\eta_f)}\left[1+\frac{12}{5}{\eta_f}^2\alpha_s g_o(4\eta_f-3)\right]+\frac{16\eta_f\alpha_s g_o(41-33\eta_f)}{15\pi}$ |

**Table 3.7:** Different expressions for the conduction coefficient.

| **Bolio *et al.* (1995)** | | | |
|---|---|---|---|
| $\lambda^* = \lambda = \frac{75}{384}\sqrt{\pi}d_P\rho_s\sqrt{T}$ | | | |
| **Hadinoto and Curtis (2004)** | | | |
| $\lambda^* = \frac{\lambda_1^*}{\lambda_1}\lambda$ | $\lambda = \frac{75}{384}\sqrt{\pi}d_P\rho_s\sqrt{T}$ | $\lambda_1 = \frac{8\lambda}{\eta_f(41-33\eta_f)}$ | $\lambda_1^* = \frac{\lambda_1}{1+\frac{6\xi_d\lambda_1}{5c_s\rho_S g_o T}}$ |

In the above relations, $\lambda$ represents the conduction coefficient for granular temperature in a vacuum and $\lambda^*$ is the modified expression when an interstitial fluid exists. Note that Bolio *et al.* (1995) use $\eta_f = (1-e_s)/2$, whereas Hadinoto and Curtis (2004) use $\eta_f = (1-e_f)/2$.

### 3.2.4 Boundary Conditions

In their simulation of fully developed pipe flow, both reference studies, i.e., Bolio *et al.* (1995) and Hadinoto and Curtis (2004), used an axisymmetric boundary condition, i.e., the gradients of all the variables are equal to zero at the centerline of the pipe. At the wall, the no-slip condition applies for the fluid and turbulence kinetic energy, and the LRN formulation determines the wall condition for the dissipation, i.e., $\varepsilon = \nu_f\,\partial^2 k/\partial r^2$. For the particle phase, the boundary conditions (3.15) and (3.16) of Johnson and Jackson (1987) are considered, which represent a partial slip condition at the wall for the mean particle velocity and an energy balance in the near wall region which determines the granular temperature at the wall.

Mean velocity:

$$\tau_{rz}^{s} = \frac{\rho_s \pi V_z \emptyset \sqrt{T}}{2\sqrt{3}\left(\frac{\alpha_o}{\alpha_s} - \frac{{\alpha_o}^{2/3}}{{\alpha_s}^{2/3}}\right)} \tag{3.15}$$

Granular temperature:

$$q_{PTr} = \frac{\sqrt{3}\rho_s \pi (1 - {e_w}^2) T^{3/2}}{4\left(\frac{\alpha_o}{\alpha_s} - \frac{{\alpha_o}^{2/3}}{{\alpha_s}^{2/3}}\right)} - \frac{\rho_s \pi V_z^2 \emptyset \sqrt{T}}{2\sqrt{3}\left(\frac{\alpha_o}{\alpha_s} - \frac{{\alpha_o}^{2/3}}{{\alpha_s}^{2/3}}\right)} \tag{3.16}$$

In the above equations, $\emptyset$ is the specularity coefficient and $e_w$ is the coefficient of restitution for particle-wall collisions. The specularity coefficient varies from 0 (for purely specular collisions on a perfectly smooth wall surface) to 1 (for completely diffuse collisions on a rough wall surface.) The specularity coefficient can be viewed as a measure of the loss of momentum of the particle in the tangential direction after a particle-wall collision.

### 3.2.5 Description of model formulations

This section offers a description of the five models used to analyze the modeling of the effects of an interstitial fluid. The main objective is to develop a group of model formulations that show a transition from the TFM developed for gas-solid flow to one that is applicable to liquid-solid flow. By evaluating the different modifications introduced, their influence on the prediction of dispersed liquid-solid flow can be assessed. Table 3.8 gives a summary of the main model features considered.

Model 1 represents the formulation of Bolio *et al.* (1995) and is used as a base model for the case of gas-solid flow. The second model formulation highlights the importance of the new expressions for the solids viscosity and granular temperature conduction coefficient when an interstitial fluid exists. The third model formulation focuses attention on the contribution of the particle fluctuating energy due to long-range inter-particle interaction as new source and sink terms, respectively, in the turbulence kinetic energy and granular temperature transport

equations. The fourth model formulation is the model of Hadinoto and Curtis (2004), while the fifth model formulation treats the long-range term as a sink of energy instead of as source, as in the fourth model. For all simulations, $e = e_s = 0.94$, $e_f = 0.5$ , $e_w = 0.5$ and $\emptyset = 0.002$ (Hadinoto and Curtis, 2004).

**Table 3.8:** Description of cases to analyze in numerical simulation.

| | **Model 1** | **Model 2** | **Model 3** | **Model 4** | **Model 5** |
|---|---|---|---|---|---|
| Model | Bolio *et al*. (1995) | Bolio modified | Bolio modified | Hadinoto and Curtis (2004) | Hadinoto modified |
| Main features | No interstitial effect | Interstitial effect for $\mu_S^*$ and $\lambda^*$ only | Interstitial effect for $\mu_S^*$ and $\lambda^*$only | Interstitial effect for $\mu_S^*$, $\lambda^*$ and all source terms | Interstitial effect for $\mu_S^*$, $\lambda^*$ and all source terms |
| Equation (2.3) | $\alpha_f \approx 1$ | $\alpha_f \neq 1$ | $\alpha_f \neq 1$ | $\alpha_f \approx 1$ | $\alpha_f \neq 1$ |
| Equation (2.5) | $\mu_S^* = \mu_s$ | $\mu_S^* = \frac{\mu_1^*}{\mu_1}\mu_s$ | $\mu_S^* = \frac{\mu_1^*}{\mu_1}\mu_s$ | $\mu_S^* = \frac{\mu_1^*}{\mu_1}\mu_s$ | $\mu_S^* = \frac{\mu_1^*}{\mu_1}\mu_s$ |
| $q_{PT}$ | $\lambda^* = \lambda$ | $\lambda^* = \frac{\lambda_1^*}{\lambda_1}\lambda$ | $\lambda^* = \frac{\lambda_1^*}{\lambda_1}\lambda$ | $\lambda^* = \frac{\lambda_1^*}{\lambda_1}\lambda$ | $\lambda^* = \frac{\lambda_1^*}{\lambda_1}\lambda$ |
| $I_k$ | $\alpha_f \neq 1$ | $\alpha_f \neq 1$ | $\alpha_f \neq 1$ | $\alpha_f \approx 1$ | $\alpha_f \neq 1$ |
| $I_T$ | $\alpha_f \neq 1$ | $\alpha_f \neq 1$ | $\alpha_f \neq 1$ | $\alpha_f \approx 1$ | $\alpha_f \neq 1$ |
| $S_{p-p}$ | 0 | 0 | $-3\varphi\beta T$ | $3\varphi\beta T$ | $-3\varphi\beta T$ |

As discussed in section 3.1, the predictions of particle fluctuations were larger than the measurements, which indicates that some energy is lost by particles due to the presence of the interstitial fluid. This suggests there should be an additional sink term in the transport equation for the granular temperature that accounts for this effect, and due to energy conservation, at the same time acting as a source term for the fluid turbulence. This effect can be achieved by

changing the sign of the term $S_{p-p}$ from positive, as originally proposed by Hadinoto and Curtis (2004), to negative. It is a major hypothesis of this thesis that this term is in fact a sink instead of a source of energy for the particle fluctuations. Due to the long distances between particles in a dilute flow, the long-range effect of particle fluctuations conveyed through the fluid is to enhance the fluid turbulence, instead of increasing the particle velocity fluctuations.

# Chapter 4: Results and Discussion

## 4.1 Single-Phase flow

The present section assesses the ability of the 1-D in-house code to predict single phase fully-developed turbulent pipe flow prior to considering multiphase flow simulations. The predicted results are compared with the results of Wu and Moin (2008), who performed DNS of turbulent single phase flow in a pipe. DNS is a useful alternative source of data compared to experimental research since it solves the complete flow field including the smallest scales of motion. The present comparison between the in-house code results and DNS data is also relevant since the in-house code includes various approximations including use of a LRN formulation to model the turbulence behavior in the near-wall region. In this context, the present section will validate the present code based on prediction of a single-phase flow.

Figure 4.1 presents the predicted results for the mean velocity normalized by the bulk velocity for a Reynolds number of $Re_D$ = 44,000. The predictions are compared to the DNS data of Wu and Moin (2008), also for $Re_D$ = 44,000, as well as the measurements of McKeon *et al*. (2004a) for $Re_D$ = 74,000 and Zagarola and Smits (1998) for $Re_D$ = 41,700. The profiles of the normalized mean fluid velocity look similar for all cases, except near the centerline, where the in-house code underpredicts the value compared to the DNS data. These observations agree with the results presented in Figure 4.2, where the velocity profile is displayed in inner coordinates, i.e., $u^+$ as function of $y^+$. The predictions of the in-house code agree with the DNS data, as well as the log-law and viscous sublayer. The conclusion obtained from Figures 4.1 and 4.2 is that the in-house code accurately predicts the mean velocity profile for a single-phase flow, with some small discrepancies in the centerline region.

Figure 4.3 shows the Darcy friction factor as a function of the Reynolds number predicted by the in-house code, the theoretical expression of Prandtl $\frac{1}{\sqrt{f}} = 2log\left(Re\sqrt{f}\right) - 0.8$, the DNS results of Wu and Moin (2008) and various experimental studies. The DNS data and experimental measurements are both closer to the theoretical result of Prandtl. Regarding the in-house code, predictions of the friction factor were at most approximately 4.5% above the values obtained from Prandtl expression. However, the error decreases as the Reynolds number increases as shown in Table 4.1. In general, these results document a reasonably good agreement between the numerical predictions and the theoretical results.

**Table 4.1:** Predicted friction factor compared to Prandtl expression results.

| $dP/dz$ (Pa/m) | $U_{bulk}$ (m/s) | $Re_D$ | $f$ (code) | $f$ (Prandtl) | Dif (%) |
|---|---|---|---|---|---|
| 450 | 1.07 | 32731 | 0.02399 | 0.02302 | 4.25% |
| 770 | 1.45 | 44379 | 0.02234 | 0.02150 | 3.88% |
| 1300 | 1.95 | 59642 | 0.02088 | 0.02007 | 4.04% |
| 2000 | 2.49 | 75997 | 0.01978 | 0.01912 | 3.47% |
| 3000 | 3.13 | 95407 | 0.01883 | 0.01819 | 3.54% |

Figure 4.4 displays the predicted normalized Reynolds shear stress obtained from the in-house code compared to the DNS data of Wu and Moin (2008) and LDV measurements of Toonder and Nieuwstadt (1997). The predicted results are in close agreement with DNS data, which shows that the LRN $k - \varepsilon$ is able to capture this profile. The difference between the numerical results and experimental measurements partially relates to the Reynolds number, i.e., the larger the value of $Re_D$, the higher the peak value of the stress.

Since Wu and Moin (2008) do not show results for the turbulence kinetic energy, Figure 4.5 presents the fluctuating velocity components in the axial and radial directions as functions of $r/R$ respectively. The in-house code calculates the turbulence kinetic energy; the fluctuating components have been approximated by the relation $u_r' = u_\theta' = u_z'/2$ following Sheen *et al.* (1993). The fluid-phase fluctuating velocities in the azimuthal and radial directions are assumed to be equal, which is an acceptable approximation in fully developed pipe flows (Kasagi and

Shikazono, 1995). For the axial component, the profile derived from the in-house code under-predicts the DNS results in the near-wall region and over-predicts them in the centerline region. On the other hand, the profile based on the in-house code overpredicts the radial component in the near-wall region, but agrees with the DNS data at the centerline. The shape of the approximate curves compared to the DNS data reflects the isotropic property of the EVM in the near-wall region, which makes the EVM unable to reproduce the near-wall anisotropy. In this context, Figure 4.5 cannot be used to validate the model predictions, but shows interesting comparisons between the DNS in-house code based on the relation of Sheen *et al.* (1993).

Equation (4.1) represents the reduced form of the streamwise momentum equation in cylindrical coordinates for fully developed incompressible turbulent single-phase flow through a smooth pipe. It can be obtained from Equation (3.1) for $\alpha_s = 0$ and including the Reynolds shear stress term (3.2).

$$\frac{-1}{\rho}\frac{\partial P}{\partial z} + \frac{\nu}{r}\frac{dU_z}{dr} + \nu\frac{d^2U_z}{dr^2} - \frac{\overline{u_z'u_r'}}{r} - \frac{d\overline{u_z'u_r'}}{dr} = 0 \tag{4.1}$$

Figure 4.6 presents the predictions of the in-house code and the DNS results of Wu and Moin (2008) for the budget components of Equation (4.1) normalized by $U_{bulk}^2/R$. Overall, the distribution of each term exhibits remarkable agreement with the DNS data for the region outside the viscous sub-layer for the pressure drop, the gradient of the viscous shear-stress, the gradient of the turbulent shear stress, the viscous shear-stress curvature and the turbulent shear-stress curvature terms, i.e.,$\frac{-1}{\rho}\frac{\partial P}{\partial x}$, $\nu\frac{d^2U_z}{dr^2}$, $-\frac{d\overline{u_z'u_r'}}{dr}$, $\frac{\nu}{r}\frac{dU_z}{dr}$ and $-\frac{\overline{u_z'u_r'}}{r}$, respectively. The pressure drop remains constant across the pipe cross section, and becomes dominant for large values of $y^+$. In the viscous sub-layer region, both the in-house code and DNS results indicate the dominant source and sink terms are the gradient of turbulent shear-stress and gradient of viscous shear-stress, respectively. The results indicate some discrepancies in the section of the curves within the viscous sublayer next to the wall. Both the DNS and in-house code predict a finite value for the viscous stress curvature and a zero value for the turbulent shear-stress curvature term at the wall.

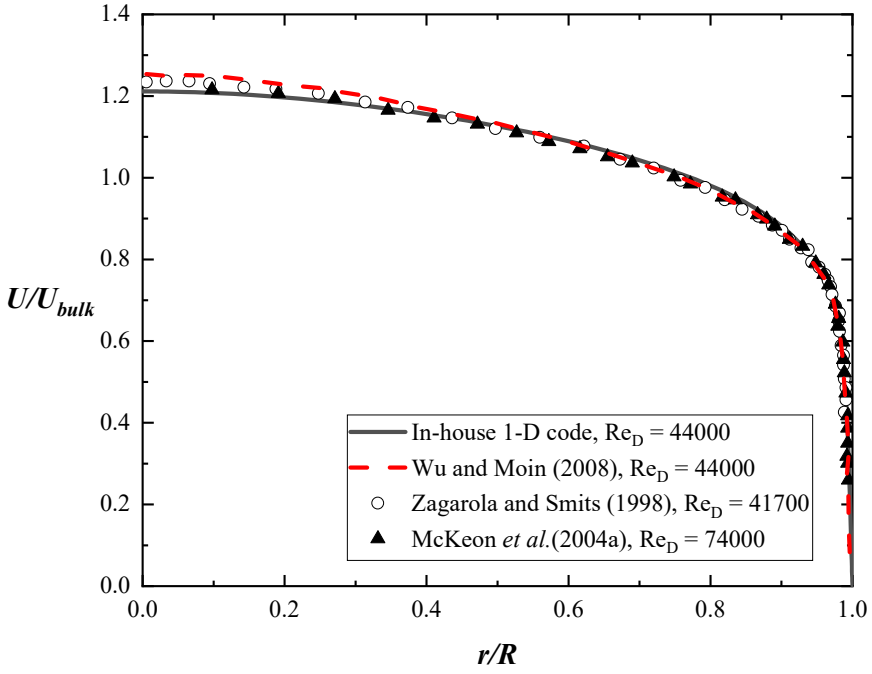


**Figure 4.1:** Numerical prediction for mean velocity in outer coordinates by the in-house 1-D code.

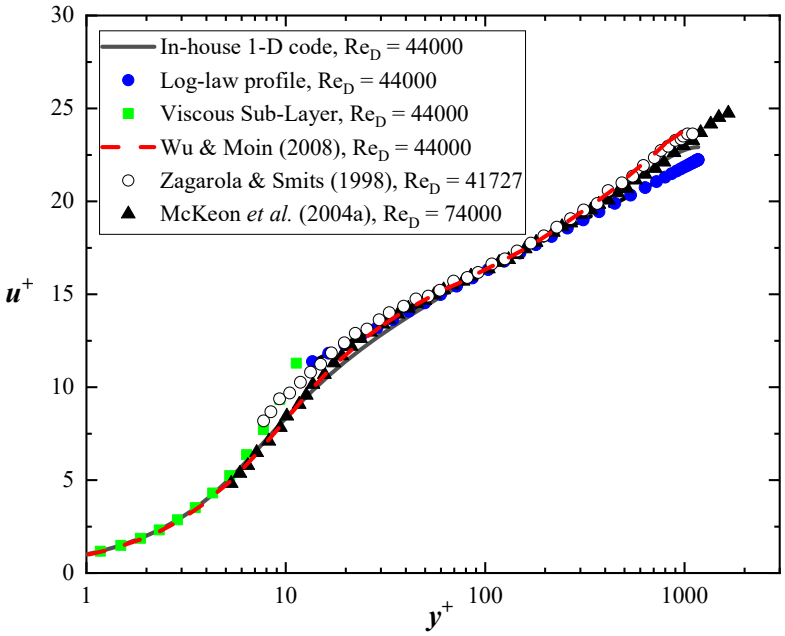


**Figure 4.2:** Predictions for mean velocity in inner coordinates by the in-house 1-D code.

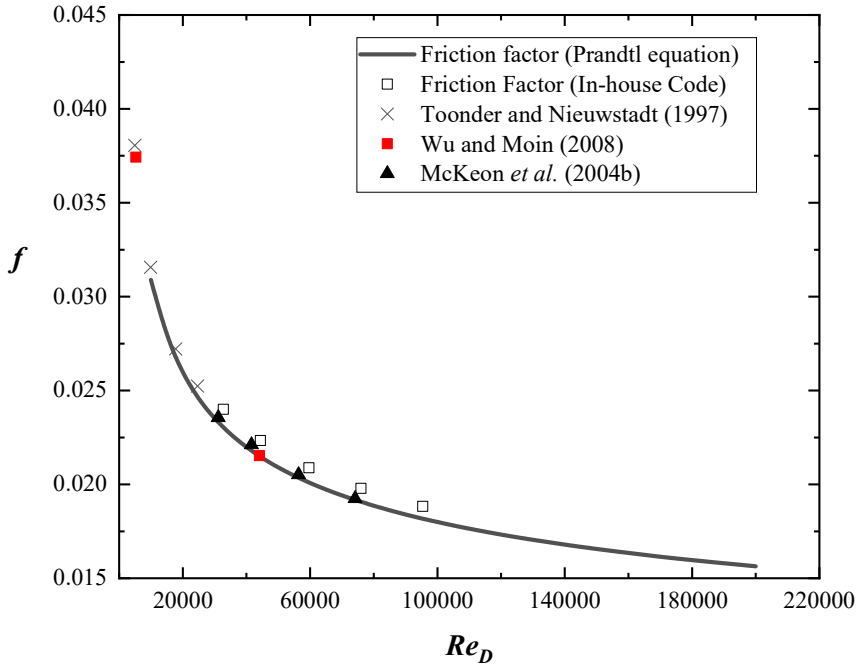


**Figure 4.3:** Friction factor $f$ predicted by 1-D in-house code and other studies.

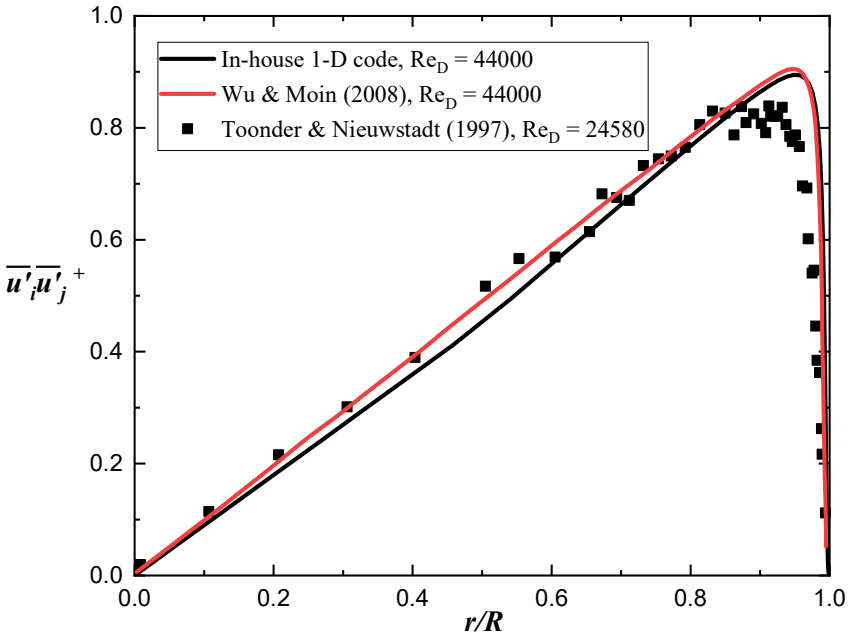


**Figure 4.4:** Normalized Reynolds shear stress as a function of $r/R$ for the 1-D code and DNS data.

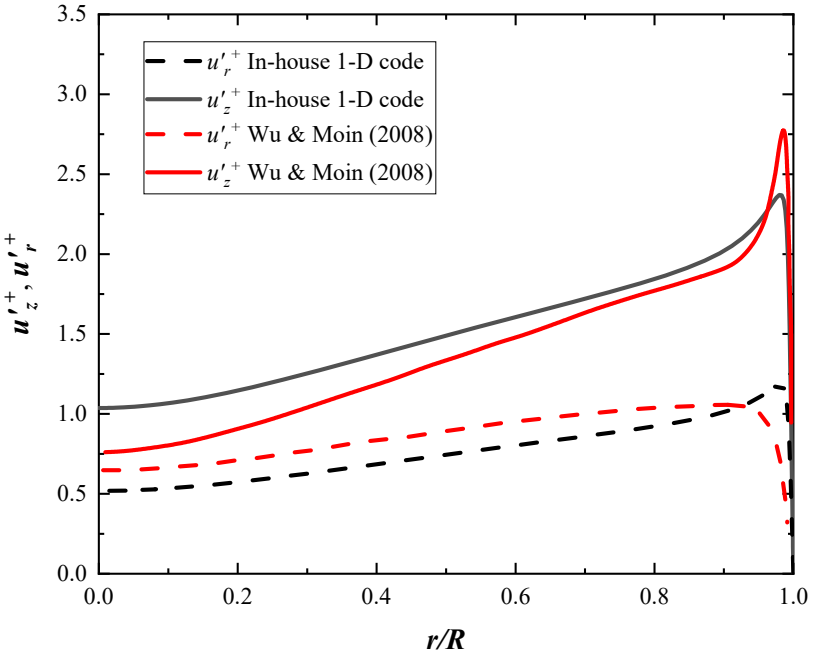


**Figure 4.5:** Normalized velocity fluctuations in the axial and radial directions as function of $r/R$ for the 1-D code and DNS data.

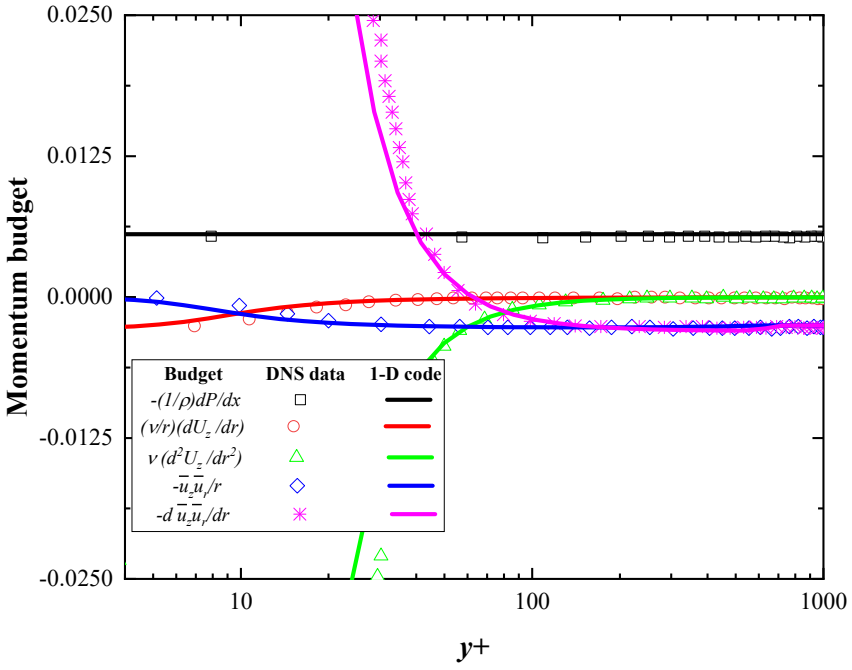


**Figure 4.6:** Predicted budget components of equation (4.1) normalized by $U_{bulk}^2/R$.

As noted above, the present section attempts to validate the in-house code by comparing its predictions with DNS data for the case of single-phase flow. Overall, the code provides reasonable predictions for the mean velocity, Reynolds shear stress, friction factor and momentum source terms. However, as expected, the eddy viscosity formulation fails to capture the anisotropy of the turbulence near the wall.

### 4.2 Prediction for liquid-solid phase flow

This section considers the predictions for fully developed liquid-solid upward flow in a vertical pipe. The equations in cylindrical coordinates (presented in previous sections) were discretized using the finite volume method of Patankar (1980). A second-order central difference scheme was used to model the diffusive term. The flow domain for the present study consists of a constant angle circular section of the flow that extends from the centerline to the pipe wall. The numerical calculations were performed using an in-house FORTRAN code that was used previously by Zaman and Bergstrom (2014) for gas-solid flow. It provides the flexibility to select, modify and implement additional functions and subroutines to simulate new terms in the transport equations. This code was modified to include the model formulations given in Table 3.8. The consideration of the interstitial fluid introduced new non-linear coefficients and source terms in the transport equations, which represented the most complex task for numerical simulation. The solution method for the set of discrete equations was the Tri-Diagonal Matrix Algorithm (TDMA) with an appropriate relaxation factor.

In order to assess the grid independence of the solutions, three different grids using $N = 60$, $N = 80$ and $N = 120$ control volumes were used for numerical simulation of a specific set of flow conditions for a particle diameter of $d_p = 2.3mm$ and $Re = 67000$. The grid was configured to achieve a high-density mesh near the wall and locate the first node in the viscous sub-layer as required by the low Reynolds number $k - \varepsilon$ model adopted. The criteria to stop the iterative calculation was when all variables achieved a normalized difference of less than 0.0001. Five variables were assessed: the volume fraction, granular temperature, turbulence kinetic energy, mean velocity of the fluid and mean velocity of the particles at three different

locations, i.e., $y^+ = 50$, $y^+ = 200$ and $y^+ = 400$. At $y^+ = 50$, the maximum change for the five variables was 3.8% when going from $N = 60$ to $N = 80$, which reduced to 1.3% when going from $N = 80$ to $N = 120$. The maximum changes found at $y^+ = 200$ and $y^+ = 400$ were 4.2% and 3.7%, respectively, when going from $N = 60$ to $N = 80$, and reduced further to 1.6% and 1.7%, respectively, when going from $N = 80$ to $N = 120$. The turbulence kinetic energy was the most sensitive variable, showing the maximum error in all cases. The maximum errors for the other variables were typically in the range of 0.2% to 0.35%. Based on the results above, a grid of $N = 80$ was used for the present study, which is consistent with the grid used by Zaman and Bergstrom (2014) as well as Bolio *et al*. (1995).

Six coupled differential equations determine the flow field. Five transport equations were used to obtain the mean velocity field of the fluid phase $U_i$ (3.1), the mean velocity field of the solid phase $V_i$ (3.3), the turbulence kinetic energy $k$ (3.8), the dissipation rate $\varepsilon$ (3.9) and the granular temperature $T$ (3.12). In addition, the radial component of the solid phase momentum equation was used to determine the volume fraction distribution $\alpha_s$ (3.4). The inputs to the FORTRAN code were the solid volume fraction at the centerline and the pressure drop. The simulations were performed by modifying the pressure drop until agreement was achieved with the total mass flow rate in the experiment. The solids volume fraction at the centerline was typically fixed, and only slightly modified in few cases to improve mass flow prediction to the experimental value. The total mass flow rate is given by:

$$w = \left(\rho_f \alpha_{f\ bulk} U_{bulk} + \rho_s \alpha_{s\ bulk} V_{bulk}\right) A \tag{4.2}$$

### 4.2.1 Mean variables

In this section, the numerical predictions are compared with the experimental data of Alajbegovic *et al.* (1994), who performed measurements using a laser-Doppler anemometer (LDA) for different cases of dilute upward liquid-solid flows in a vertical pipe of 30.6 mm diameter with bulk solids volume fractions ranging from 1% to 4%. Water was the carrier phase and two types of solid particles were used as the dispersed phase, i.e., ceramic and expanded polystyrene. The pipe wall was smooth. Measurements of the mean local velocities, solids

volume fraction, fluctuating solid and fluid velocities, and fluid and solid shear stress were obtained. The gamma-ray technique was used for the concentration measurements. The present section first analyzes the predictions for a specific mass flow rate of $w$ = 1.469 kg/s using ceramic particles. Later, the predictions for two additional mass flow rates are presented. The case of expanded polystyrene particles was not studied due to the fact that it requires additional modifications to the code to include the virtual mass effect, which is relevant for flows with small density ratios. The carrier and dispersed phase properties are listed in Table 4.2.

**Table 4.2:** Mixture properties from Alajbegovic *et al.* (1994).

| **Properties** | **Carrier Phase** | **Dispersed Phase** | |
|---|---|---|---|
| Material | Water | Ceramic | Expanded Polystyrene |
| Density $\rho$ (kg/m$^3$) | 997.1 | 2442.9 | 31.91 |
| Viscosity $\mu$ (kg/s · m) | 0.001 | - | - |
| Diameter $d_p$ (mm) | - | 2.32 | 1.79 |

The behavior of the particles is governed by the Stokes number $S_T = \tau_P/\tau_f$. Table 4.3 shows the results for $S_T$ predicted for each model, as well as the experimental range reported by Hadinoto and Curtis (2004) for the experiment of Alajbegovic *et al.* (1994). The predictions for all models are relatively similar with variations within a range of 2.4 %. The predicitons are also within the experimental range.

**Table 4.3:** Stokes number.

| | **Model 1** | **Model 2** | **Model 3** | **Model 4** | **Model 5** | **Experimental** |
|---|---|---|---|---|---|---|
| $S_T$ | 45.5 | 45.5 | 46.2 | 46.6 | 46.3 | 40-90 |

For a flow with $S_T \ll 1$ the particles respond very quickly to any change in the flow field and therefore are able to follow the path of the fluid elements. This type of flow can be analyzed as single-phase. In the present case $S_T \gg 1$, which means that the particles do not immediately respond to changes in the flow field and therefore do not follow the path of the fluid elements. Therefore, a single-phase analysis is not appropriate, and coupling effects need to be considered

through the application of more complex models such as the TFM and KTGF.

Figure 4.7 displays the predicted mean velocity profile for both phases, i.e., solid and liquid, for the five model formulations presented in Table 3.8. The predictions for the fluid mean velocity are almost identical for the five formulations, whereas larger discrepancies exist for the solid mean velocity. For the fluid phase, Model 3 performs the best, i.e. is closer to the experimental data overall. The next best prediction is given by Model 5, which marginally underpredicts the mean fluid velocity in the core section. For the solid phase, all models under-predict the velocity profile when compared to the experimental data. Model 3 and Model 5 both give the closest agreement to the experimental data at the centerline, however, Model 5 performs better near the wall. For all models, the solid mean velocity predictions exhibit a change in curvature near the wall. The location of the inflection point is close to the location where particle velocity becomes larger than the fluid velocity based on the experimental data, which implies a change of direction in the particle drag force, i.e., $F_D = \beta(U - V)$. All of the model formulations predict a finite velocity at the wall, which is consistent with the trend of the experimental data.

Figure 4.8 shows the results for the solids volume fraction profile. All cases share a similar value at the centerline, which is close to the experimental value. For models 1, 2 and 3, there is a consistent reduction in the predicted value at the wall, which is due to the inclusion of the interstitial fluid effects through the new formulations of $\mu_S^*$ and $\lambda^*$ (Model 2), and the addition of the term $S_{p-p}$ (Model 3). The overall reduction in the predicted value of $\alpha_s$ at the wall from Model 1 to Model 3 is approximately 70%. Although not capturing the exact shape of the measurements, the profile for Model 3 does capture the trend of $\alpha_s$ as the wall is approached. Finally, moving from Model 4 to Model 5 also improves the prediction for $\alpha_s$. Model 5 shows the best agreement with the experimental data in the core region, but over-predicts the results at the wall compared to Model 3. In both cases, the predicted results support the hypothesis that the sign of $S_{p-p}$ should be such as to account for the enhanced turbulence kinetic energy due to the particle fluctuations. The bulk solid volume fractions for the different model formulations in Table 4.4 shows that the profiles with a reduced value near the wall also have lower bulk values.

**Table 4.4:** Consolidated bulk solid volume fraction.

| | **Model 1** | **Model 2** | **Model 3** | **Model 4** | **Model 5** |
|---|---|---|---|---|---|
| $\boldsymbol{\alpha_s}$ | 0.0498 | 0.0404 | 0.0254 | 0.0403 | 0.0326 |

A noticeable characteristic of the experimental data for the solids volume fraction is that it reduces to approximately zero at the wall, which implies there are no particles next to the wall. The drag and gravity forces are the main factors that influence the particle motion in the axial direction, i.e., Equation (3.3). However, because of the velocity gradient and turbulence of the fluid, additional forces on the particle are also present, e.g., the lift force, wall lubrication force, virtual mass, history force and buoyancy force. Some of these forces result in motion in the radial direction. For example, the lift force directs particles toward the centerline due to the fluid velocity gradient. These radial forces tend to keep particles away from the wall, which explains why the experimental measurements show a peak of $\alpha_s$ at the centerline and a zero value at the wall.

Figures 4.9 and 4.10, respectively, present the turbulence kinetic energy $k$ normalized by $J_L^2$ and the granular temperature $T$ normalized by $J_S^2$, where $J_L = \alpha_f U_{bulk}$ is the fluid superficial velocity and $J_S = \alpha_s V_{bulk}$ is the solids superficial velocity. For Figure 4.9, the single-phase results are also included for comparison purposes. For the numerical simulations, $k$ and $T$ are calculated by the in-house code; however, the experimental values of $k$ and $T$ were reconstructed from the measurements of the axial and radial velocities of each phase using the approximation $u_r' = u_\theta'$ (Sheen *et al*., 1993, Shikazono, 1995). The reason for reconstructing the values of $k$ and $T$ from the velocity components is that the eddy viscosity model is inherently unable to predict the anisotropic behavior of the turbulence motion at the wall. From Table 4.5 is it evident that the predicted values of $J_L$ are very similar and within 3.9% of the experimental measurement. However, larger differences occur for the predicted values of $J_S$, with Model 3 being closest to the experimental value. The value of $J_S$ depends on the model formulation, and the effect of the new interstitial formulations is to bring Model 3 closer to the experimental value.

**Table 4.5:** Fluid and solid superficial velocities.

| | **Model 1** | **Model 2** | **Model 3** | **Model 4** | **Model 5** | **Exp. Data** | **Single-Phase** |
|---|---|---|---|---|---|---|---|
| $\boldsymbol{J_L(\mathrm{m/s})}$ | 1.815 | 1.835 | 1.891 | 1.879 | 1.882 | 1.888 | 1.888 |
| $\boldsymbol{J_S(\mathrm{m/s})}$ | 0.077 | 0.068 | 0.045 | 0.067 | 0.058 | 0.045 | - |

The predictions for the turbulence kinetic energy in Figure 4.9 indicate that Model 3 performs the best in the core region. Moving from Model 1 to 3, the turbulence level is reduced in the core region and increases slightly in the near-wall region. Overall, the profile for Model 3 is closest to the experimental data in the core region of the flow. In contrast, Models 4 and 5 over-predict the turbulence across the entire pipe cross section, which is due to the contribution of the additional source terms included in $S_{k,IT}$ to enhance the fluid turbulence. All models predict a peak at the same location near the wall, in agreement with the experimental data. This represents the production due to the interaction of the mean velocity gradient and the Reynolds shear stress, which is a dominant feature of turbulent near-wall flow. Surprisingly, the single-phase results show good agreement with the experimental data, which suggests that for this specific flow the turbulence enhancement in the model may be calibrated to a single-phase value that is too high. On the other hand, it is not clear from the measurements whether the particles have indeed resulted in turbulence enhancement.

The predictions for the granular temperature in Figure 4.10 indicate that Models 3 and 5 give the best predictions in the core region, but over-predict the experimental results in the near-wall region. In contract, Model 1 over-predicts the profile in the core region, but is close to the experimental profile near the wall. Regardless of Model 1 results, which perform better agreement at the wall, this result is because of the overprediction of $J_S$ instead of an accurate prediction of $T$ and $J_S$. The improved predictions for the granular temperature in the core region for Model 3 and 5 is due to including $S_{p-p}$ as a sink term in the granular temperature equation. The remaining two model formulations, Model 2 and 4, over-predict the profiles across the entire pipe.

It is insightful to point out a connection between Figures 4.10 and 4.8. Irrespective of model, the profile of $T$ initially increases when moving from the centerline towards the wall, and then at some point direction begin to slowly decrease up to the wall. The opposite trend occurs for the profile of $\alpha_s$ ; it begins with a peak value at the centerline and then decreases towards the wall, finally turning upward and increasing in value up until the wall. The inflection behavior for both profiles, i.e., $T$ and $\alpha_s$, is the same for each model. Equations (3.6) and (3.4), which are used to solve $\alpha_s$, explain this behavior. In equation (3.6) $T$ and $\alpha_s$ are inversely proportional, which means that when $T$ increases, then $\alpha_s$ decreases, and viceversa.

Figure 4.11 represents a comparison of the predicted fluid Reynolds stress profiles for each model formulation and the experimental measurements. For all simulations, the location of the peak point is similar. In all cases, the profile is over-predicted compared to the experimental data, especially in the near-wall region. There is no significant change from Model 1 to 3 and from Model 4 to 5. However, the over-prediction of Models 4 and 5 is much higher compared to the other model formulations.

Figure 4.12 compares the predictions for the normalized eddy viscosity profiles for each case. The profiles clearly show how the turbulence is attenuated when moving from Model 1 to 3, i.e., when the interstitial fluid effects are included in the base model developed for gas-solid flow. For Models 4 and 5, the predictions for the eddy viscosity are much higher than for the other models, especially in the core region. The reduction in the turbulence level between Model 4 and 5 is due to the term $S_{p-p}$, which acts as a source term in Model 5 in the transport equation of $k$. In general, Models 3 and 5 clarify the effect on the turbulence enhancement of the interstitial source terms in $S_{k,IT}$ included in the model of Hadinoto and Curtis (2004).

Finally, Figures 4.13 and 4.14 present the normalized results for the turbulence kinetic energy and the Reynolds shear stress, respectively, i.e., $k^+ = k/u_\tau^2$ and $-\overline{u_1'u_2'}^+ = -\overline{u_1'u_2'}/u_\tau^2$ using inner coordinates. The calculated values of the friction velocity $u_\tau$ for each model formulation are listed in Table 4.6.

**Table 4.6:** Consolidated fluid superficial velocities.

| | **Model 1** | **Model 2** | **Model 3** | **Model 4** | **Model 5** | **Single-Phase** |
|---|---|---|---|---|---|---|
| $u_\tau$ **(m/s)** | 0.1040 | 0.1021 | 0.1025 | 0.1104 | 0.1076 | 0.0968 |

The predictions for the friction velocity, $u_\tau$, are relatively similar in all cases. A lower value for $u_\tau$ implies a lower pressure gradient for the same mass flow rate. The largest variation is approximately 8.1% and occurs for models 2 and 4. The small reduction from Model 1 to Model 2 reflects the impact of the new formulations for $\mu_S^*$ and $\lambda^*$. In general, the results shown in Figure 4.13 and 4.14 agree with those in Figures 4.9 and 4.11, respectively.

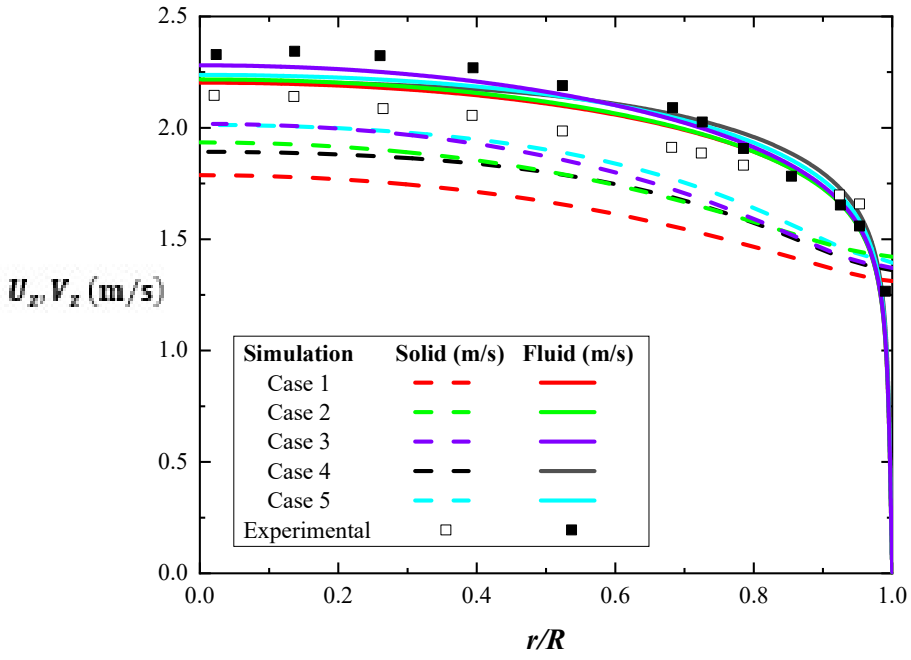


**Figure 4.7:** Comparison of the axial mean fluid and solid velocities with the experimental data of Alajbegovic *et al*. (1994).

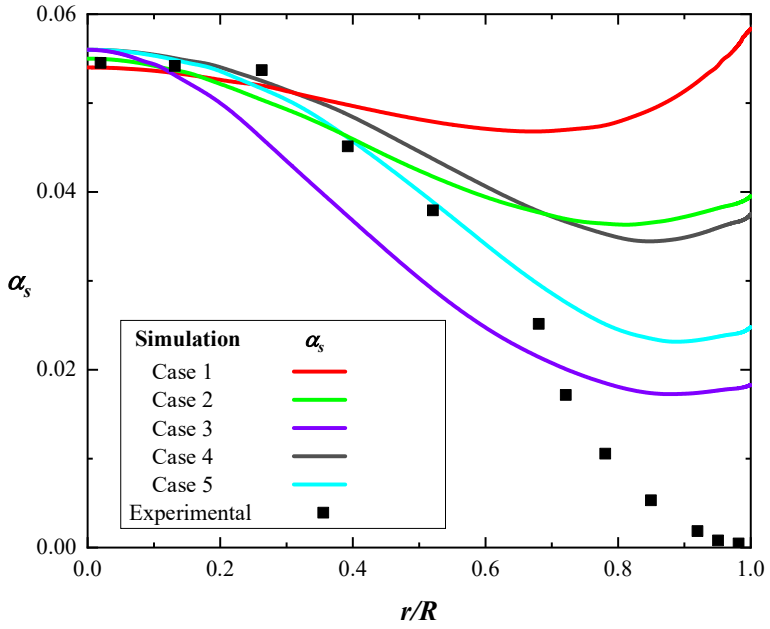


**Figure 4.8:** Comparison of the solids volume fraction predictions and the experimental data of Alajbegovic *et al*. (1994).

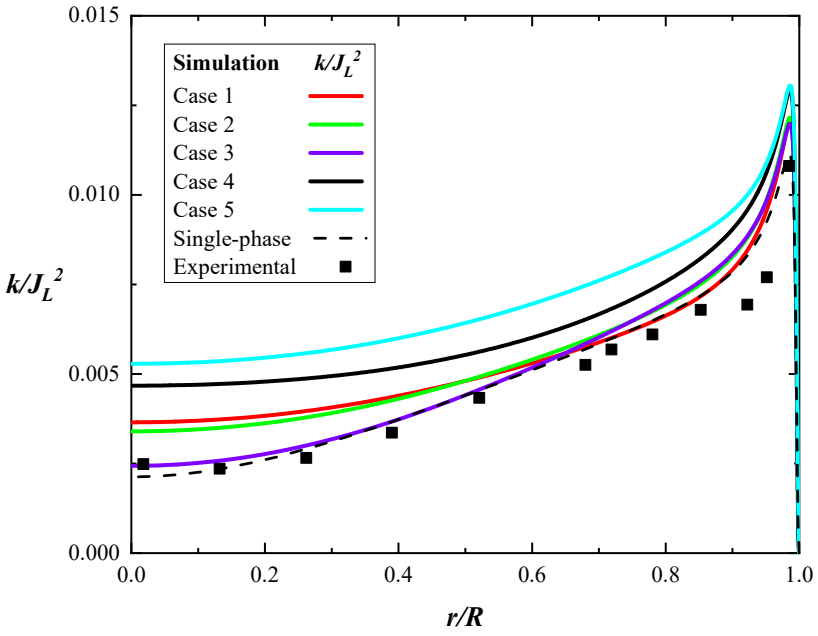


**Figure 4.9:** Predicted turbulence kinetic energy $k$ and the experimental data of Alajbegovic *et al.* (1994) normalized by $J_L^2$.

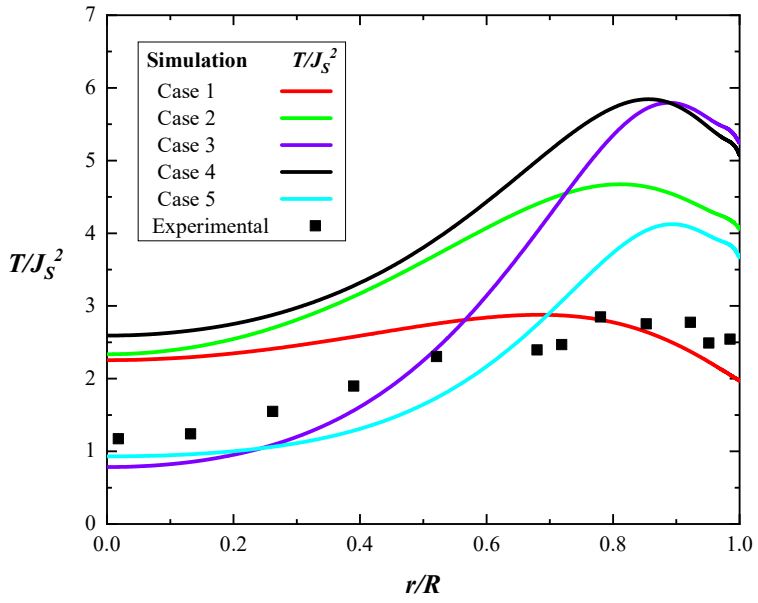


**Figure 4.10:** Predicted granular temperature $T$ and the experimental data of Alajbegovic *et al*. (1994) normalized $J_S^2$.

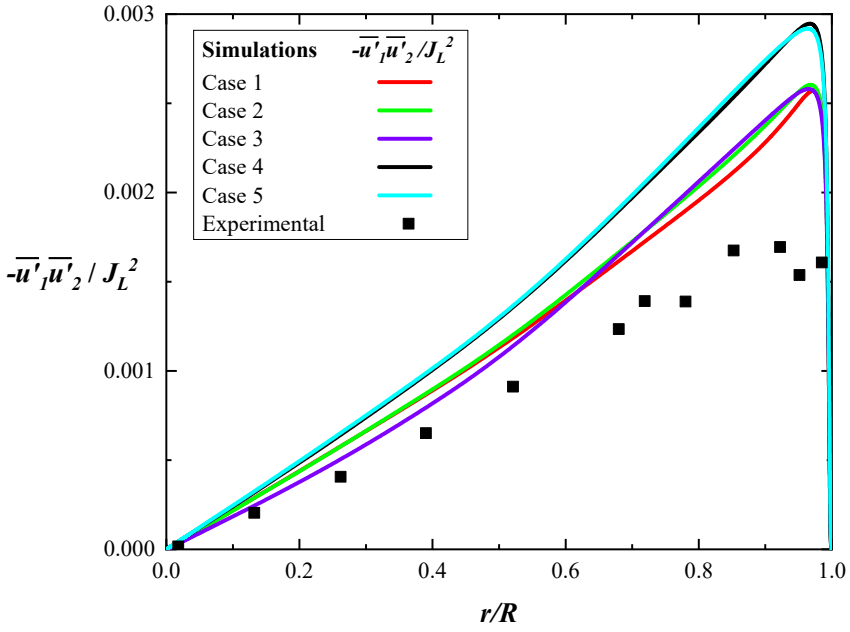


**Figure 4.11:** Predicted Reynolds shear stress $-\overline{u_1'u_2'}$ and the experimental data of Alajbegovic *et al*. (1994) normalized by $J_L^2$.

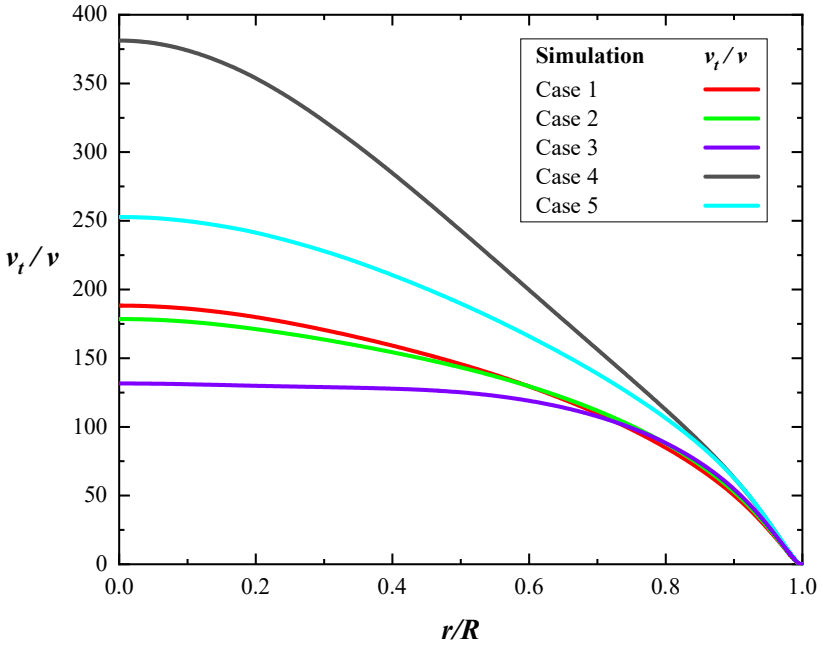


**Figure 4.12:** Comparison of the turbulent viscosity predictions.

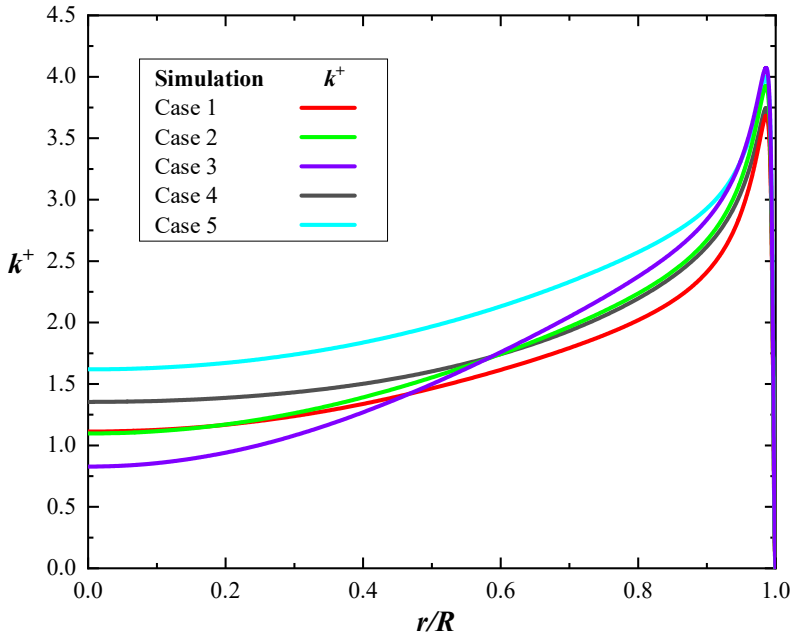


**Figure 4.13:** Comparison of the predictions for the turbulence kinetic energy using inner-coordinates.

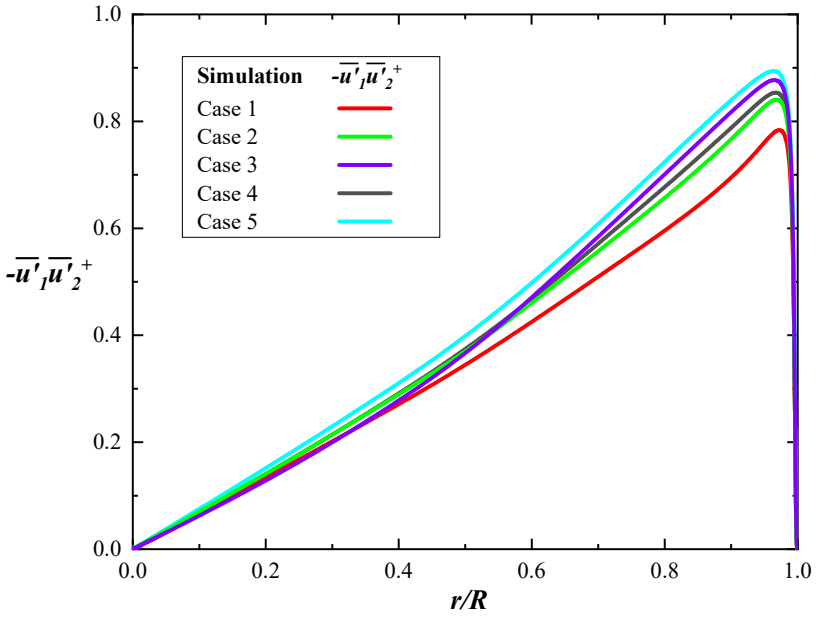


**Figure 4.14:** Comparison of the predictions for the fluid Reynolds shear stress using inner coordinates.

### 4.2.2 Balance of transport equations for *k* and *T*

This section examines the source terms in the transport equations for the granular temperature and turbulence kinetic energy as predicted by Models 1, 3 and 5. The main objective is to compare the base case formulation, Model 1, for gas-solid flow, to models that better perform in terms of the predictions for the granular temperature and turbulence kinetic energy in a liquid-solid flow. The results will be presented using a semi-log scale to highlight the rapid changes that occurs in the region closest region to wall, i.e., within the viscous sub-layer $y^+ < 10$. Note that the figures in this section indicate the source terms that exist in the regular gas-solid model by black curves and the additional source terms included in liquid-solid model by red curves.

Figures 4.15, 4.16 and 4.17 present the source terms for the transport equation for the granular temperature. The first comparison will be between Models 1 and 2, based on the results

in Figure 4.15 and 4.16. The figures use different scales on the vertical axis to highlight the difference in magnitudes of the source terms for each model. Note that the main reason Model 1 performs differently than Model 3 is due to the new formulations for $\mu_S^*$ and $\lambda^*$and the addition of $S_{p-p}$, which is zero in Model 1. These modifications diminish the particle fluctuations in the outer region of the pipe cross section (see Figure 4.10) by reducing the magnitude of the source terms. The production term $P_T$ is reduced dramatically in going from Model 1 to 3, e.g., the peak value around $y^+ \approx 200$ decreased by 75 %. Also, $P_T$ becomes dominant in the outer region $y^+ > 150$ for both models; however, it becomes negligible in the viscous sub-layer for $y^+ < 10$. For Model 1, $P_T$ is balanced by diffusion $D_T$ in the log-law region, whereas for Model 3 it is compensated by both $D_T$ and $S_{p-p}$. The diffusion term $D_T$, as well as $P_T$, reduces significantly in magnitude from Model 1 to 3, e.g., the value of $D_T$ at the wall drops by around 50%. For both Models 1 and 3, $D_T$ is the main source of energy for particle fluctuations in the viscous sub-layer. However, further away from the wall it becomes negative, and finally becomes positive again around $y^+ \approx 850$ in Model 1 and $y^+ \approx 500$ in Model 3. The dissipation term due to particle collisions $\gamma$ is generally small, and reduces to almost zero going from Model 1 to Model 3. These results agreed with the expectations, i.e., in a gas-solid flow it is expected to have a much higher particle-particle collision frequency compared to liquid-solid flow. Similarly, collision velocities in a gas-solid flow are likely to be much higher compared to liquid-solid flow, due to the liquid viscosity being three orders of magnitude larger than for a gas. The higher viscosity significantly increases the kinetic energy dissipated when particles move freely between collisions, represented by the new term $S_{p-p}$. Regarding the modulation term $I_T$, for Model 1 it varies from a negative contribution in the viscous sub-layer, to a positive value in the log-law region and finally becomes negative in the outer region. This implies that in the outer region, the destruction due to the drag force dominates over the production due to interaction between fluctuating velocity fields; this reverses in the log-law region. For Model 3 the contribution of the modulation term is positive for both the log-law and outer regions, which indicates the predominance of particle energy generation due the interactions between particle and fluid fluctuations. For both Models 1 and 3, $I_T$ becomes large and negative in the viscous sub-layer, where it balances the positive contribution of diffusion.

Figure 4.17 presents the results of Model 5, which is the model of Hadinoto and Curtis (2004), but differs from it by considering $S_{p-p}$ as a sink of granular energy instead of a source as proposed originally. The source terms are similar in shape for Model 3 and 5, however, for Model 5 the magnitude is almost twice that for Model 3. For both models, the dissipation term $\gamma$ is almost zero, which implies a negligible energy dissipation due inelastic particle-particle collisions.

The role of diffusion in a granular flow may be challenging to understand physically at the beginning. A simple approach is to recall that the KTGF is the application of the principles of the kinetic theory of gases to solid particles, treating them as if they were molecules. In this context, the role of diffusion can be understood easily by making an analogy to a pipe with a gas flowing through it. More specifically, it is possible to make an analogy between the pseudo-thermal energy term $q_{PT} = -\lambda^*(\omega G_{3K} + G_{3c})\frac{\partial T}{\partial r}$ and the conductive heat transfer flux $q = -\kappa\frac{\partial \psi}{\partial r}$, where $\kappa$ is the conductivity coefficient and $\psi$ is the thermal temperature. Just as the spatial gradient of thermal temperature determines the direction of the heat flux, the gradient of granular temperature determines the direction of the transfer of particle fluctuating energy. Furthermore, since the term $\lambda^*(\omega G_{3K} + G_{3c})$ is always positive, like the thermal conductivity coefficient $\kappa$, the positive or negative direction developed by $q_{PT}$ is due to the gradient of $T$ in the radial direction. When a fluid develops a viscous sub-layer at the wall, there is no turbulent transport in this region and the thermal energy is transferred by "conduction", referred to as diffusion in fluids. Diffusion is the transfer of energy by random motion of particles. This analogy helps to explain why the source term $D_T$ is predominant in the viscous-sub layer. From the profiles presented in Figure 4.10, there is a peak of $T$ near the wall, and $T$ decreases when approaching the wall. Assuming a similar profile for the thermal temperature $\psi$, would imply a heat flux from the gas to the wall. The amount of heat transferred from the gas to the wall is a boundary condition, which for a granular flow is represented by $q_{PTr}$ . The coefficient of restitution at the wall $e_w$ plays an important role in the determining the diffusion and granular temperature profiles.

Figures 4.18, 4.19 and 4.20 document the contributions of the various source terms in the

transport equation for the turbulence kinetic energy for Models 1, 3 and 5, respectively. Again, the scale of the vertical axis on the plots is different in order to accommodate the different magnitude of the source terms for each model. As for the granular temperature, the source terms for Model 1 differ from those for Model 3 in terms of $\mu_S^*$, $\lambda^*$ and $S_{p-p}$. For both Models 1 and 3, similar peak values of production and dissipation, i.e., $P_K \approx 25$ and $\varepsilon \approx -25$, occur just outside the viscous sub layer at $y^+ \approx 10$. In addition, the value of the dissipation at the wall is practically the same, i.e. $\varepsilon_w \approx 12.5$, for both models, and $P_K$ becomes negligible both near the wall and in the outer region. On the other hand, the modulation term $I_k$ changes dramatically from Model 1 to 3 because of the term $S_{p-p}$. For Model 1, $I_k$ is positive in the viscous sub-layer, becomes negative in the log-law region and then positive again in the outer region; whereas for Model 3, the modulation is only positive in the viscous sub-layer and elsewhere negative. For Model 1, the diffusion term $D_K$ balances the contribution of $I_K$ over most of the pipe cross section, whereas for Model 3, $D_K$ balances the contribution of $S_{p-p}$. The $S_{p-p}$ term is zero for Model 1, however it becomes the dominant energy source for fluid turbulence across the entire the pipe cross section for Model 3. The highest value of $S_{p-p} \approx 75$ occurs at the wall, while the lowest value $S_{p-p} \approx 12$ occurs at $y^+ \approx 10$. The effect of $S_{p-p}$ is opposite in Figures 4.19 and 4.16, for the fluctuating fluid and particle velocities, respectively. This behavior of the fluid turbulence and particle fluctuations agrees with the physical interactions expected: the energy extracted from the particle fluctuations increases the fluid turbulence. It is possible to observe a similar behavior between $I_k$ and $I_T$ , with small differences in the magnitudes.

Lastly, Figure 4.20 presents the predicted results for Model 5. The scale of the vertical axis is 4 times higher than for Figure 4.19 due to an increase in the magnitude of each source term because of the larger contributions of $E_W$ and $S_{p-p}$. The turbulence kinetic energy balance for Model 5 includes new source terms which were zero in Models 1 and 3, i.e., the contribution due to wakes $E_W$, generation due to the collisional fluid stress $G$ and particle-collisions $\gamma_{FKET}$. The wake term $E_W$ and $S_{p-p}$ represent the maximum and second largest source of fluid turbulence, respectively, outside the viscous sub-layer. These terms generate an enhancement of $k$ in the pipe core region, in agreement with the prediction shown in Figure 4.9. This model

outcome is based on the formation of vortex shedding due to wakes behind particles for value of the particle Reynolds number $R_p$ larger than 300 (Lun, 2000). At the same time, an enhanced fluid turbulence increases the particle fluctuations. Although the generation of wakes is a well known physical feature in particle-fluid flows, determining an appropriate formulation to model it is still a challenge. The formulation of $E_W$ used by Hadinoto and Curtis (2004) was developed for a gas-particle flow (Lun, 2000), where wakes can be generated more readily than in a liquid, again due to the significant difference in viscosity between both fluids. The contributions of the other terms, i.e., $G$ and $\gamma_{FKET}$, are almost negligible, which makes $E_W$ and $S_{p-p}$ the main sources in modifying the distribution of the turbulence kinetic energy. The diffusion term $D_K$ balances both $E_W$ and $S_{p-p}$, as well as $I_k$. Due to the dominance of $E_W$ in Model 5, its implementation has a strong effect on the granular temperature, turbulence kinetic energy and volume fraction profiles.

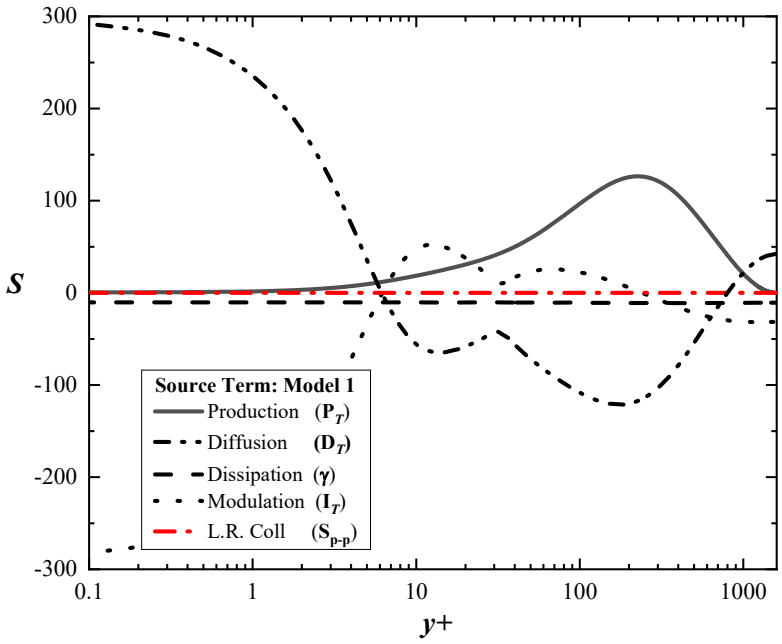


**Figure 4.15:** Source terms for the granular temperature equation predicted by Model 1.

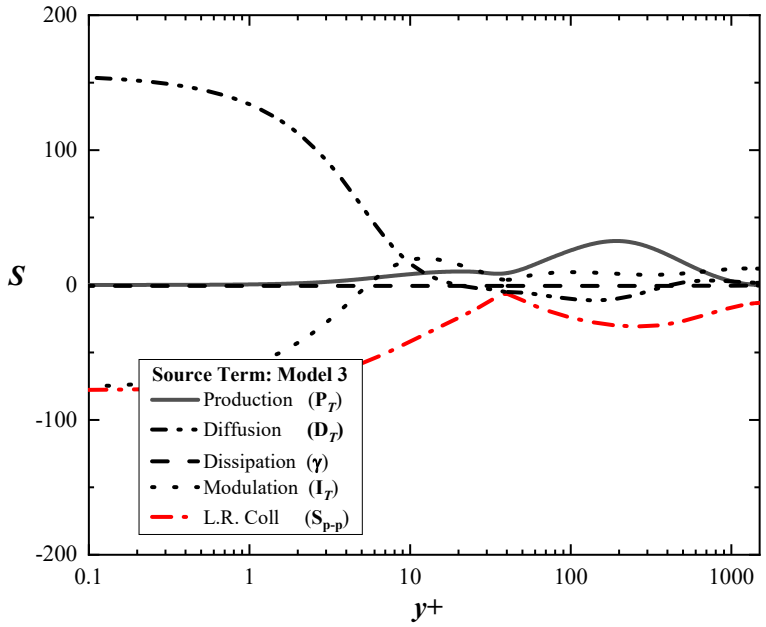


**Figure 4.16:** Source terms for the granular temperature equation predicted by Model 3.

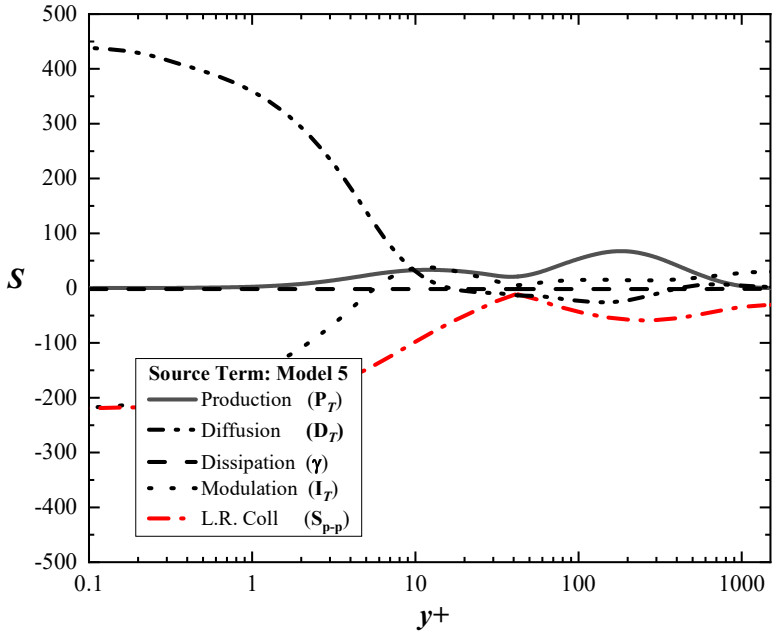


**Figure 4.17:** Source terms for the granular temperature equation predicted by Model 5.

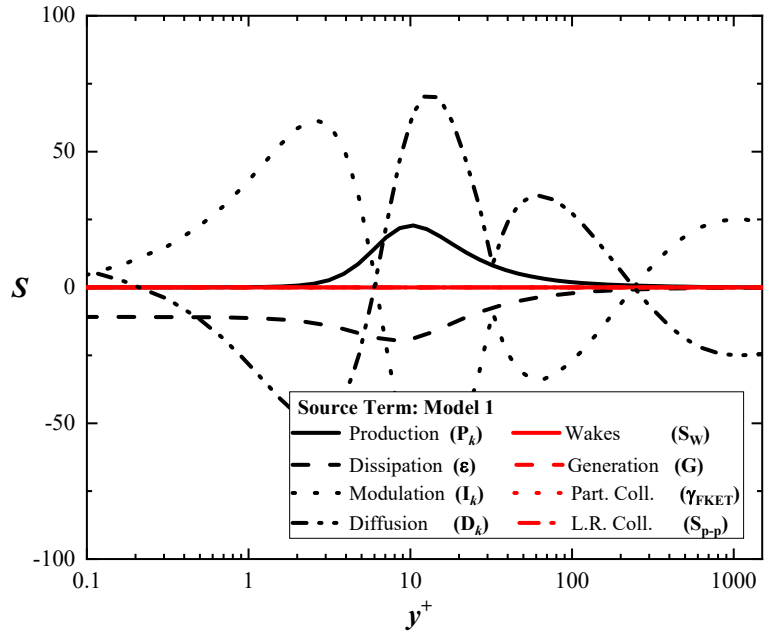


**Figure 4.18:** Source terms for the turbulence kinetic energy equation predicted by Model 1.

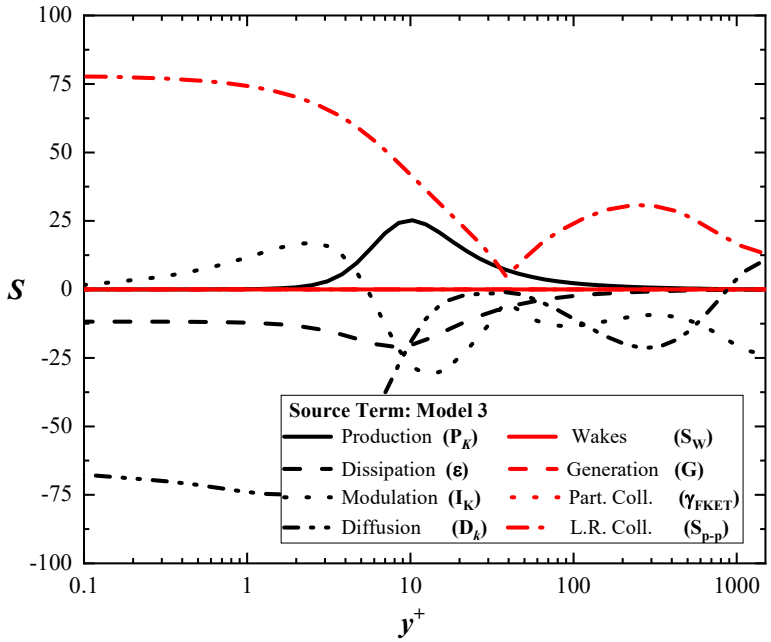


**Figure 4.19:** Source terms for the turbulence kinetic energy equation predicted by Model 3.

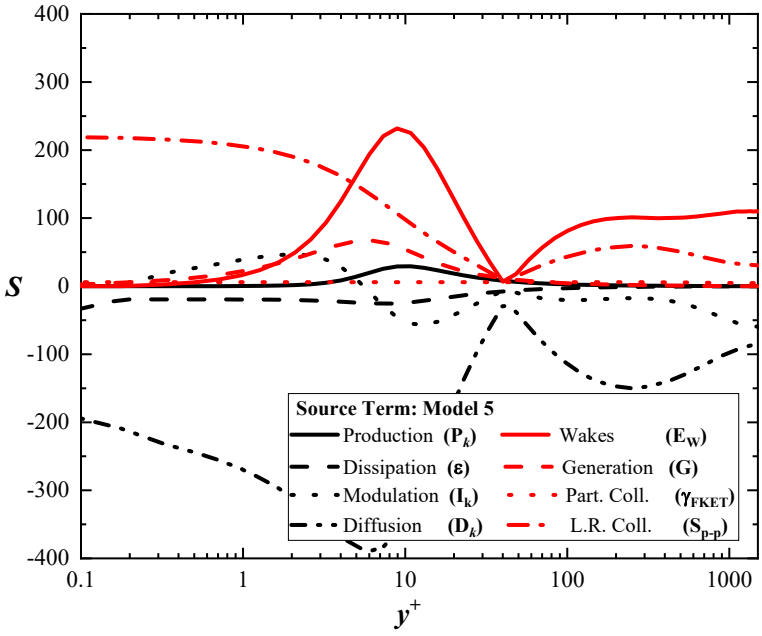


**Figure 4.20:** Source terms for the turbulence kinetic energy equation predicted by Model 5.

### 4.2.3 Predictions for different flow rates

In this section, the numerical predictions are obtained using Model 3 for all three different mass flow rates, i.e., $w$ = 1.095 kg/s, $w$ = 1.469 kg/s and $w$ =1.723 kg/s, considered in the experimental study of Alajbegovic *et al.* (1994). The measurements considered the same flow conditions, i.e., upward flow in a vertical pipe 30.6 mm in diameter, water as the carrier phase and ceramic particles ($\rho_s = 2443\ \mathrm{kg/m^3}$, $d_p = 2.32\mathrm{mm}$) as the dispersed phase. In general, the predictions showed the same level of agreement with the experimental data as documented in section 4.2.1 for all the variables analyzed, with the exception of the solids volume fraction and normalized granular temperature for $w$ = 1.095 kg/s. The predicted values of the fluid ( $J_L$ ) and solid ( $J_S$ ) superficial velocities were very close to the measured values as will be shown in the figures below.

Figure 4.21 shows the predicted mean axial velocities for the liquid and solid phases. For

the liquid phase, the predictions show close agreement with the experimental data for all mass flow rates, especially in the near-wall region. In addition, the relative velocity $U_r = U_z - V_z$ at the centerline remains almost constant for the three cases analyzed. At some point when moving from the centerline towards the wall, $U_r \rightarrow 0$ and the mean fluid velocity becomes slower than the solids mean velocity. The location where this occurs, i.e. where $U_r = 0$, moves further away from the wall as total mass flow rate *w* increases. The predicted solids velocity profile shows less agreement with the experimental data. The simulations predict a finite velocity at the wall, based on the boundary condition defined for this phase in Equation (3.15). Note that the experimental measurements are not close enough to the wall to confirm whether the experimental value of the particle velocity was also finite at the wall. The difference between the measured and predicted mean particle velocities increases when moving towards the wall for all mass flow rates. These observations suggest that the interfacial drag coefficient and the boundary conditions of Johnson and Jackson (1987) may need to be revised in order to improve their application in liquid-solid flows.

Figure 4.22 presents the volume fraction predictions for the different mass flow rates. For all three mass flow rates analyzed, the volume fraction at the centerline matches the experimental data, and generally decreases as the wall is approached. For the case of *w* = 1.095 kg/s, the lowest mass flow rate, the experimental $\alpha_s$ profile first shows a gradual increase up to *r/R* = 0.5 and then decreases rapidly to zero when approaching the wall. In general, the model still over-predicts the volume fraction results in the vicinity of the wall, while the experimental measurements indicate $\alpha_{wall} = 0$ at the wall.

Figures 4.23 and 4.24 show the predictions for the turbulence kinetic energy and the granular temperature normalized by the fluid and particle superficial velocities, respectively. As mentioned in the discussion of Figures 4.9 and 4.10, the measured turbulence kinetic energy and granular temperature were reconstructed from the axial and radial velocities measurements using the approximation $u_r' = u_\theta'$ (Sheen *et al*., 1993, Shikazono, 1995). For the turbulence kinetic energy profiles shown in Figure 4.23, close agreement between predictions and experimental data is obtained across the entire pipe cross section. The largest difference occurs for the case of *w* = 1.095 kg/s. Both the predicted and measured profiles increase as the total

mass flow rate decreases. This effect is less noticeable at the centerline, but is clearly manifest by the peak values located near the wall for both the predicted results and the experimental data.

For the granular temperature, Figure 4.24 shows that the agreement between the experimental data and predictions improves in the core region, while some level of over-prediction occurs near the wall for $w$ = 1.723 kg/s and $w$ = 1.469 kg/s, a similar trend to that observed in Figure 4.10. For $w$ = 1.095 kg/s, the predicted results show much larger differences with the experimental data across the pipe, which is similar to the predictions for the solid volume fraction predictions. This is consistent with the direct relation between these two properties based on the model relations. In spite of this phenomenon, the predictions are able to follow the same trend as the experimental data, i.e., a smooth increase when moving from the centerline of the pipe to the wall, followed by a peak value and finally a smooth decrease in the near-wall region.

Figure 4.25 shows the prediction for the Reynolds shear stress normalized by the superficial fluid velocity. The predictions are in close agreement with the measurements in the core region, but over-predict the results in the near-wall region, especially near the peak. The level of agreement between the experimental data and predicted results appears to increase as the mass flow rate increases.

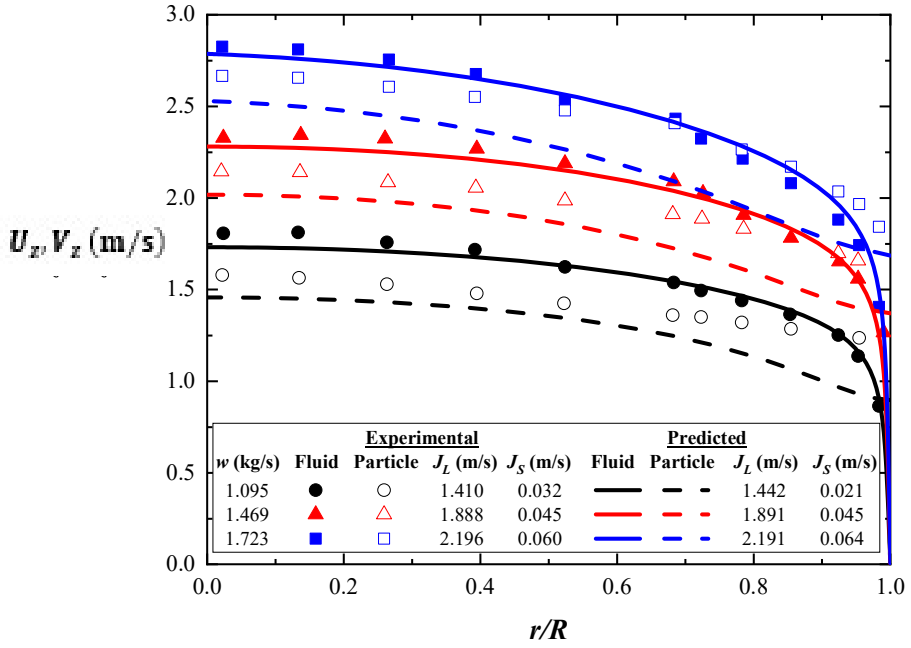


**Figure 4.21:** Predicted and experimental mean velocity profiles for fluid and particle phases.

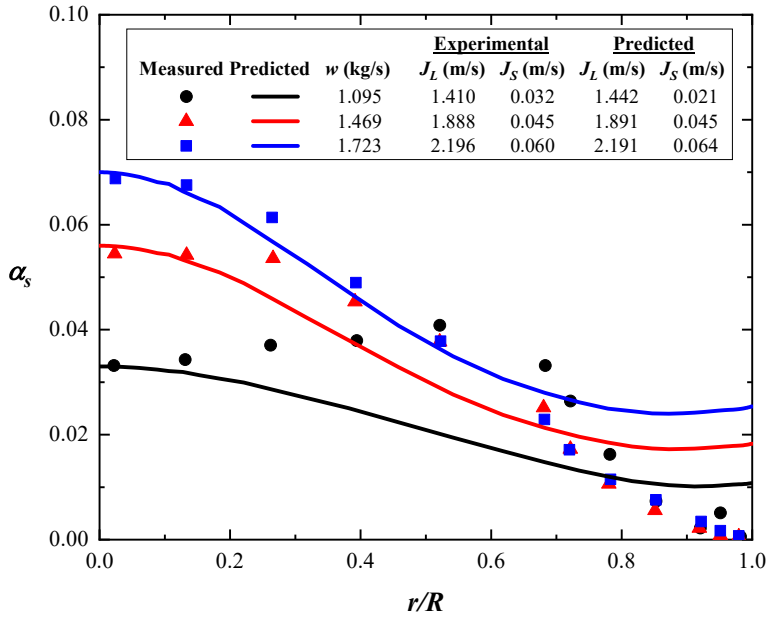


**Figure 4.22:** Measured and predicted solid volume fraction profiles for the liquid and particle phases.

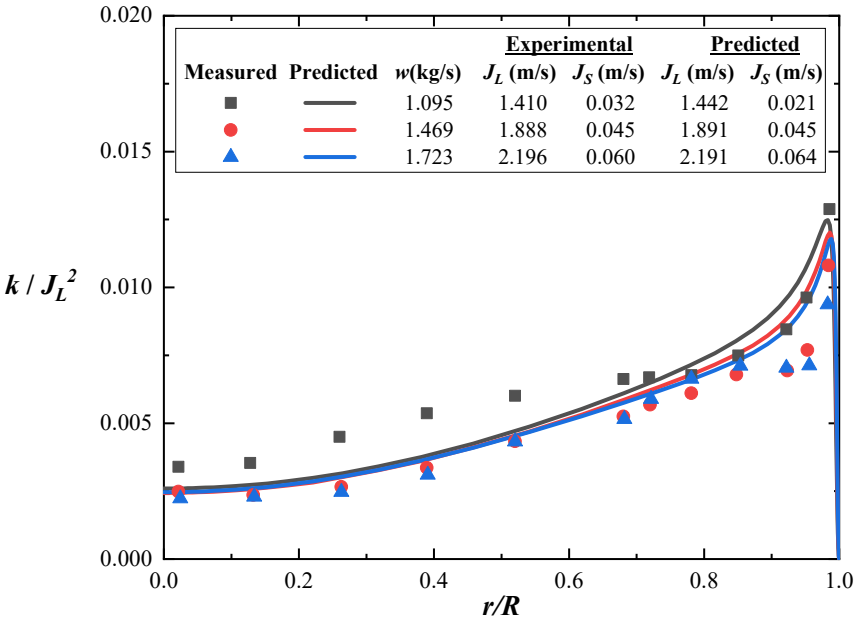


**Figure 4.23:** Measured and predicted turbulence kinetic energy profiles for normalized by $J_L^2$.

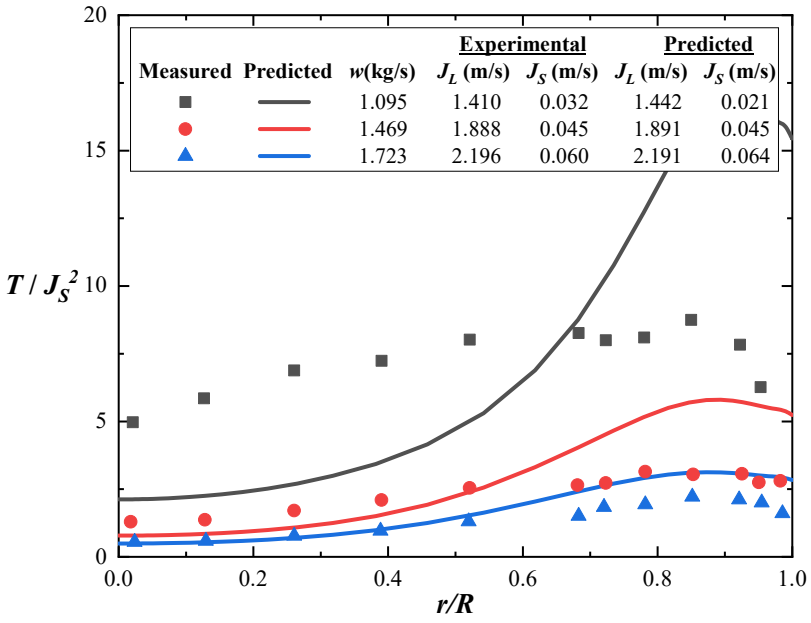


**Figure 4.24:** Measured and predicted profiles of the granular temperature $T$ normalized by $J_S^2$.

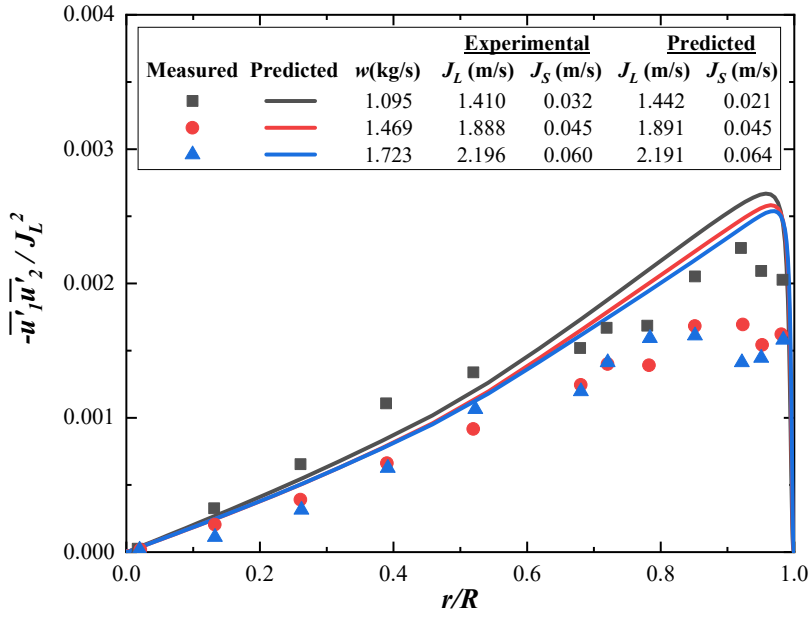


**Figure 4.25:** Measured and predicted profiles for the Reynolds shear stress normalized by $J_L^2$.

In general, the numerical predictions of the velocity profiles for both the solid and liquid phases agree with the experimental values for all mass flow rates. However, this behavior does not extend to the other variables, e.g., the solids volume fraction, turbulence kinetic energy, granular temperature, and Reynolds shear stress. In the case of those variables, the agreement with the experimental data varies with the mass flow rate: the largest discrepancies occur for the lowest mass flow rate.

# Chapter 5: Summary and Conclusions

## 5.1 Summary of simulations

The present work began with an extensive literature review focused on the differences between TFM and KTGF formulations for gas-solid and liquid-solid flows. Three test models were generated based on the addition and/or modification of specific terms to reproduce the physics of liquid-solid flow. To analyze the predictions of each model, numerical simulations were performed using an in-house code. First, the code was validated for single-phase fully-developed turbulent flow in a pipe using DNS data. Subsequently, an extensive set of simulations were performed to assess the three test models and two other reference models based on comparison to experimental measurements of a mixture of water and ceramic particles. Finally, the model that overall best matched the experimental results was evaluated for a range of mass-flow rates.

The present dissertation shows the importance of including interstitial fluid effects for simulation of liquid-solid flows. This study highlights the relevance of the new formulations for the solid viscosity and granular temperature conductive coefficient, as well as the contributions of the long-range interaction term $S_{p-p}$ and the wake term $E_W$. Otherwise, it suggests that the contribution of the turbulence source terms related to the collisional fluid stress $G$ and particle collisions $\gamma_{FKET}$, included in $S_{k,IT}$, are negligible. Although the generation of wakes by particles in a fluid needs to be considered, the intensity of vortex shedding is different in a gas than in a liquid for the same size of particle.

## 5.2 Single-phase flow

Numerical simulations of single-phase flow were performed to validate the performance of the in-house code. Predictions were compared to the DNS data of Wu and Moin (2008) and some additional experimental measurements. The simulations were performed using the LRN $k-\varepsilon$ model of Myong and Kasagi (1990) to model the turbulence and its behavior in the near-wall region.

In general, the predicted results were in close agreement with the DNS data for the mean velocity in outer and inner coordinates, the friction factor, the Reynolds shear stress and the source terms of the momentum equation (4.1). The mean velocity predictions, both in inner and outer coordinates show good agreement with the DNS results and experimental data. Some differences occur in the centerline region, where the predicted results were slightly lower. As shown in Table 4.1, the predictions for the friction factor are slightly larger (< 4.5%) than the theoretical curve. Another important outcome is the close agreement between the predicted Reynolds shear stress and the DNS values. The discrepancy with the experimental measurements occur due to the different values of the Reynolds number, i.e., the predicted results are for a larger value of $Re_D$ compared to the experimental measurements, which is reflected in a higher peak value near the wall. The prediction for the momentum transport equation also shows good agreement with the DNS data for all of the individual terms in the momentum equation, which demonstrates the capability of the in-house code to reproduce the physical behavior of the fluid in the near-wall region.

For the fluctuating axial and radial velocities, some discrepancies were found in terms of the profile shape and peak values near the wall, as well as the value of the axial fluctuating velocity at the centerline. These discrepancies relate to the use of an eddy viscosity for the Reynolds stress tensor. The in-house code calculates the turbulence kinetic energy $k$, and then uses an eddy viscosity model to estimate the components of the Reynolds stress tensor. The approximation of the fluctuating velocity components was based on the assumptions of Sheen *et al.* (1993) and Shikazono (1995), i.e., $u_r' = u_\theta' = u_z'/2$. These approximations fail near the

wall, where the peak values of the three fluctuating velocity components are highly anisotropic. Given the deficiency in the use of an eddy viscosity model for the Reynolds stress, the multiphase flow sections compare the predicted values of $k$ to a profile reconstructed from the measurements of the fluctuating velocity using the assumption $u_r' = u_\theta'$.

Overall, the in-house code has demonstrated the capability to well predict the single phase flow. Predictions of the mean velocity, isotropic turbulence parameters, Reynolds shear stress, friction factor and momentum transport equation components are reasonably close to the DNS and experimental data used for comparison. These results validated the performance of the in-house code prior to its application to multiphase-flows.

### 5.3 Multiphase Flow

The present research compares the performance of the Two Fluid Model developed by Bolio *et al.* (1995) for gas-solid flow, and the models of Hadinoto and Curtis (2004) and Hadinoto (2010) in predicting liquid-solid flow. Three intermediate model formulations were developed to incorporate different model components related to the effect of the interstitial fluid, with the intention to study their specific effect on the liquid-solid flow predictions. Results for each model, assuming a smooth surface, were compared and documented with the experimental measurements performed by Alajbegovic *et al.* (1994) for dispersed liquid-solid turbulent flow in a vertical pipe. Overall, the intermediate Model 3, which is a modified version of the model of Bolio *et al.* (1995) that includes new formulations for $\mu_S^*$ and $\lambda^*$, as well as the source term $S_{p-p}$, showed the best predictions for the liquid and solid mean flow properties compared to the other models. The predictions for the turbulence kinetic energy and the granular temperature were also improved for the case of Model 3. The predictions show that this model is capable of including an interstitial fluid effect that increases the turbulence kinetic energy due to the particle fluctuations through the term $S_{p-p}$. Lastly, it is able to follow the trend of the solid volume fraction experimental data, which shows a smooth decrease when moving towards the wall. The effect of particle wakes is included in Models 4 and 5. Only Model 5 results in improved agreement between the mean velocity and granular temperature predictions and the

experimental measurements in the core region, however the turbulence kinetic energy is over-predicted. Model 5 considered the term $S_{p-p}$ as a sink of energy for the granular temperature and source of energy for the turbulence kinetic energy, as did Model 3.

The modification and/or addition of some terms in the gas-solid model to include the effect of the interstitial fluid, improves the prediction of the solids volume fraction profile: the predicted value at the wall reduces by about 70% for Model 3 compared to Model 1. These results compared to the experimental data indicate that interstitial fluid effects may become more important when approaching the wall. The main differences between Models 1 and 2 principally relates to the new versions of the solid viscosity $\mu_S^*$ and granular temperature conductive coefficient $\lambda^*$, and avoiding simplifications due to the low solids volume fraction in the transport equations, e.g., neglecting the fraction of the fluid pressure drop in the particle momentum equation $\alpha_s \frac{\partial P_f}{\partial z}$ for $\alpha_s \approx 0$. In a vertical pipe, this fraction relates to the buoyancy force on a particle, which becomes relevant when the particle is surrounded by a liquid, but can be neglected in a gas. In general, retaining this term implies the contribution of the pressure drop in the fluid and solid momentum equations depends on the solids volume fraction level, instead of applying the total pressure drop to the fluid equation as in Model 1. The same occurs for the drag coefficient, whose original version developed by Wen and Yu (1966) is a function of the product of the solid and fluid volume fractions, instead of only the solid volume fraction.

Another aspect of the present research is the inclusion of the long-range interaction between particles through the fluid term $S_{p-p}$ in Model 2 as an energy sink of the granular temperature transport equation and as an energy source in the turbulence kinetic energy transport equation, represented as Model 3. This approach is opposite to the original proposal of Hadinoto and Curtis (2004); however, the simulations have demonstrated an improvement in the agreement with the experimental data. Hadinoto and Curtis (2004) suggested that particles transmit and increase their fluctuating energy by long-range interactions between them through the interstitial fluid, represented by the term $S_{p-p}$. However, the hypothesis of the present research is that the term $S_{p-p}$ does not represent a source of particle fluctuating energy, but rather a sink. In a dilute flow, where the distance between particles is typically large compared to their

diameters, the particle velocity fluctuations generate additional turbulence in the fluid from a long-range perspective, which is dissipated by the fluid before another particle can feel it. In addition, fluid-particle interactions are expected to differ in gas-solid and liquid-solid flow cases. The larger density and molecular viscosity of a liquid compared to a gas may imply lower particle-particle collision frequencies and lower collision velocities. This in turn suggests that the granular temperature dissipation through inelastic particle-particle collisions should be considerably lower for liquid-solid flow compared to gas-solid flow. This reasoning agrees with the granular temperature source terms predicted by Model 3 and plotted in Figure 4.16, which shows that the source of the granular temperature $T$ in the log-law and outer regions is mainly due to production $P_T$ and interactions with the fluid fluctuating velocity field given by the modulation term $I_T$. The sink or destruction of the granular temperature is mainly due to the $S_{p-p}$ term and the diffusion $D_T$, with a very small contribution due to the inelastic particle-particle collision $\gamma$. In the viscous sub-layer, $D_T$ is the main source term of $T$ and the sink term is mainly due to $S_{p-p}$ and $I_T$. The term $S_{p-p}$ could be interpreted as a modulation term due to the fact that it exchanges energy between the fluid and particle fluctuation fields.

From a balance of the source terms of the granular temperature equation, the diffusion term plays an important role, especially in the viscous sub-layer. This accords with the principles of the kinetic theory of gases, as it explains the transfer of thermal energy for gas flow in a pipe. The addition of the new term $S_{p-p}$ in turn dramatically changes the magnitudes of the other source terms, as can be observed in Figure 4.16 compared to Figure 4.15; however, the shape remains similar and diffusion remains dominant in the viscous sub-layer. Overall, the models based on the KTGF are not able to reproduce some important features of the experimental data, e.g., the correct level of the particle velocity and the zero solids volume fraction at the wall. As pointed out previously, there is a close relationship between the value of $\alpha_s$ and $T$, hence, improving predictions for one variable would imply better predictions of the other.

The analysis of the five model formulations was performed with the intention to evaluate the contribution and relevance of each new source term with respect to the experimental measurements. For example, for the budget of the turbulence kinetic energy, the behavior of

the production and dissipation rate terms changed in magnitude, but retained the same shape as for single-phase flow even with the addition of new source terms, as can be noticed in Figure 4.18 to Figure 4.20. Based on the budget analysis for the $T$ and $k$ transport equations, it can be concluded that the turbulence modulation and the new term $S_{p-p}$ are dominant, and contribute to closer agreement with the experimental measurements, whereas the terms due to collisional fluid stress $G$ and particle collisions $\gamma_{FKET}$ are negligible.

Based on a careful analysis of the predictions for the mean variables and budget terms, Model 3 gave the closest agreement with the experimental data. The final part of the study examined its performance for different mass flow rates (or mass loadings). The results were mixed. The predictions for the mean velocities were consistent for all mass flow rates. However, other variables, such as the granular temperature, showed a dependence on the mass flow rate: the discrepancy between the predicted values and measurements increased as the mass flow rate decreased. Similar discrepancies were observed for other variables, which may indicate a deficiency is the present model formulations.

### 5.4 Future work

The present research has identified the following topics that could be addressed in the future to further advance the TFM for prediction of liquid-solid flows:

1. Investigation of novel models to better predict the wake effect in liquid-solid flow, opposed to using formulations developed for gas-solid flow.
2. The implementation of improved boundary conditions. The popular model of Johnson and Jackson (1987) was developed for gas-solid flow, but as was demonstrated in the present work, liquid-solid flow includes addition physics, which may imply the need for modification of the boundary conditions.
3. The need to develop an improved formulation for the $S_{p-p}$ term and the drag coefficient $\beta$ for applications in liquid-solid flows.

4. The lack of agreement between the predicted solids volume fraction profile and the experimental measurements in the near-wall region suggests that solving the solids volume fraction profile from the particle pressure equation may not be appropriate. A more complete assessment of the radial force balance for the solids phase may be required.
5. The additional forces characterizing the liquid-particle interaction, such as virtual mass, which are neglected in the present work may be important for different flows, such as when the particle density is much lower.
6. The anisotropy of the turbulence in the wall region requires the use of a second-moment closure. This would also have significant implications for the turbulence modulation terms.
7. The present study clearly shows that the granular temperature is insufficient to include all of the particle fluctuations. The turbulent motions of the particles would be better predicted using an appropriate turbulence model, such as the eddy viscosity approach based on a $k-\varepsilon$ model for the particle field. A relevant reference is the study of Krampa (2009).
8. In dense slurries, a higher solids volume fraction generates contact between particles, which develops frictional forces that are not considered in a dilute case. The additional stresses generated by friction forces must be analyzed to extend the capabilities of simulation for dense slurries.

# REFERENCES


Alajbegović, A., Assad, Bonetto, & Lahey. (1994). Phase distribution and turbulence structure for solid/fluid upflow in a pipe. *International Journal of Multiphase Flow*, 20(3), 453-479.

Anderson, T., & Jackson, R. (1967). Fluid Mechanical Description of Fluidized Beds. Equations of Motion. *Industrial & Engineering Chemistry Fundamentals*, 6(4), 527-539.

Armenio, V., Piomelli, & Fiorotto. (1999). Effect of the subgrid scales on particle motion. *Physics of Fluids*, 11(10), 3030-3042.

Batchelor, G., & Green, J. (1972). The determination of the bulk stress in a suspension of spherical particles to order c 2. *Journal of Fluid Mechanics*, 56(3), 401-427.

Bolio, E., Yasuna, J., & Sinclair, J. (1995). Dilute turbulent gas-solid flow in risers with particle-particle interactions. *AIChE Journal*, 41(6), 1375-1388.

Brennen, C. (2005). *Fundamentals of multiphase flow*. Cambridge; New York: Cambridge University Press.

Cao, J. and Ahmadi, G. (1995). Gas-particle two-phase turbulent flow in a vertical duct. *Int. J. Multiphase Flow*, 21(6):1203–1228.

Chen, H., & Patel, V. (1988). Near-wall turbulence models for complex flows including separation. *AIAA Journal*, 26(6), 641-648.

Chen, P., Sanyal, J., & Dudukovic, M. (2004). CFD modeling of bubble columns flows: Implementation of population balance. *Chemical Engineering Science*, 59(22-23), 5201-5207.

Chu, K., Wang, B., Yu, A., & Vince, A. (2009). CFD-DEM modelling of multiphase flow in dense medium cyclones. *Powder Technology*, 193(3), 235-247.

Comer Jr., J.K. (1998). *Computational two-phase flow analyses and applications to gas-liquid and gas-solid flows*. PhD. Thesis, North Carolina State University, North Carolina.

Crowe, C. (2000). On models for turbulence modulation in fluid–particle flows. *International Journal of Multiphase Flow*, 26(5), 719-727.

Crowe, C., Schwarzkopf, J., Sommerfeld, M., & Tsuji, Y. (2012). *Multiphase flows with droplets and particles*. Boca Raton, Fla.: CRC Press.

Crowe, C., Sommerfeld, M, & Tsuji, Y. (1998). *Multiphase flows with droplets and particles*. Boca Raton, Fla.: CRC Press.

Cundall, P., & Strack, O. (1979). A discrete numerical model for granular assemblies. *Géotechnique*, 29(1), 47-65.

Das, A. (2018). *Numerical analysis of turbulent gas-solid flows in a rough horizontal channel using the eulerian two-fluid model*. MSc Thesis, Department of Mechanical Engineering, University of Saskatchewan, Saskatoon, Canada.

Den Toonder, J., & Nieuwstadt. (1997). Reynolds number effects in a turbulent pipe flow for low to moderate Re. *Physics of Fluids*, 9(11), 3398-3409.

Ding, J., & Gidaspow, D. (1990). A bubbling fluidization model using kinetic theory of granular flow. *AIChE Journal*, 36(4), 523-538.

Drew, D. (1983). Mathematical Modeling of Two-Phase Flow. *Annual Review of Fluid Mechanics*, 15(1), 261-291.

Drew, D., & Passman, S. L. (1999). *Theory of multicomponent fluids* (Applied mathematical sciences (Springer-Verlag New York Inc.); v. 135). New York: Springer.

Durbin, P. A., Medic, G., Seo, J. M., Eaton, J. K., & Song, S. (2001). Rough Wall Modification of Two-Layer k-$\varepsilon$. *Journal of Fluids Engineering*, 123(1), 16-21.

Ekambara, K., Sanders, R., Nandakumar, K., & Masliyah, J. (2009). Hydrodynamic Simulation of Horizontal Slurry Pipeline Flow Using ANSYS-CFX. *Industrial & Engineering Chemistry Research*, 48(17), 8159-8171.

Ekambara, K., & Dhotre, M. (2010). CFD simulation of bubble column. *Nuclear Engineering and Design*, 240(5), 963-969.

Ekambara, K., Nandakumar, K., & Joshi, J. (2008). CFD Simulation of Bubble Column Reactor Using Population Balance. *Industrial & Engineering Chemistry Research*, 47(21), 8505-8516.

Elghobashi, S. (1991). Particle laden-turbulent flows: Direct simulation and closure models. *App. Sci. Res*., 48(3-4):91–104.

Elghobashi, S. (1994). On predicting particle-laden turbulent flows. *Applied Scientific Research*, 52(4), 309-329.

Enwald, H., Peirano, E., and Almsted, A. E. (1996). Eulerian two-phase flow theory applied to fluidization. *Int. J. Multiphase Flow*, 22(Suppl.):21–66.

Frawley, P., O'Mahony, A.P., & Geron, M. (2010). Comparison of Lagrangian and Eulerian simulations of slurry flows in a sudden expansion. (Author abstract)(Report). *Journal of Fluids Engineering*, 132(9), 091301 (12).

Gidaspow, D. (1994). *Multiphase flow and fluidization:Continuum and kinetic theory descriptions with applications*. Boston: Academic Pres.

Gillies, R. G. (1993). *Pipeline Flow of Coarse Particle Slurries*. PhD Thesis, Department of Chemical Engineering, University of Saskatchewan, Saskatoon, Canada.

Gondret, P., Lance, & Petit. (2002). Bouncing motion of spherical particles in fluids. *Physics of Fluids*, 14(2), 643-652.

Gore, R., & Crowe, C. (1989). Effect of particle size on modulating turbulent intensity. *International Journal of Multiphase Flow*, 15(2), 279-285.

Hadinoto, K. (2010). Predicting turbulence modulations at different Reynolds numbers in dilute-phase turbulent liquid–particle flow simulations. *Chemical Engineering Science*, 65(19), 5297-5308.

Hadinoto, K., & Curtis, J. (2004). Effect of Interstitial Fluid on Particle−Particle Interactions in Kinetic Theory Approach of Dilute Turbulent Fluid−Particle Flow. *Industrial & Engineering Chemistry Research*, 43(14), 3604-3615.

Haghgoo, M., Bergstrom, D., & Spiteri, R. (2018). Effect of particle stress tensor in simulations of dense gas–particle flows in fluidized beds. *Particuology*, 38, 31-43.

Hamidipour, M., Chen, J., & Larachi, F. (2012). CFD study on hydrodynamics in three-phase fluidized beds—Application of turbulence models and experimental validation. *Chemical Engineering Science*, 78, 167-180.

Hashemi, S., Sadighian, A., Shah, S., & Sanders, R. (2014). Solid velocity and concentration fluctuations in highly concentrated liquid–solid (slurry) pipe flows. *International Journal of Multiphase Flow*, 66, 46-61.

Hiltunen K., Jasberg A., Kallio S., Karema H., Kataja M., Koponen A., Manninen M. & V. Taivassalo. (2009). *Multiphase Flow Dynamics - Theory and Numerics*. Number 722 in VTT Publications.

Hosokawa, S., & Tomiyama, A. (2004). Turbulence modification in gas–liquid and solid–liquid dispersed two-phase pipe flows. *International Journal of Heat and Fluid Flow*, 25(3), 489-498.

Hrenya, C., Bolio, E., Chakrabarti, D., & Sinclair, J. (1995). Comparison of low Reynolds number k− ε turbulence models in predicting fully developed pipe flow. *Chemical Engineering Science*, 50(12), 1923-1941.

Ishii, M., & Originating Research Org. Not Identified. (1975). *Thermo-fluid dynamic theory of two-phase flow*. France: Eyrolles, Paris, France.

Ishii, M., Hibiki, Takashi. author, & SpringerLink. (2006). *Thermo-Fluid Dynamics of Two-Phase Flow*.

Jenkins, J., & Savage, S. (1983). A theory for the rapid flow of identical, smooth, nearly elastic, spherical particles. *Journal of Fluid Mechanics*, 130(-1), 187-202.

Johnson, P., & Jackson, R. (1987). Frictional-collisional constitutive relations for granular materials, with application to plane shearing. *Journal of Fluid Mechanics*, 176, 67-93.

Johnson, P., Nott, P., & Jackson, R. (1990). Frictional–collisional equations of motion for participate flows and their application to chutes. *Journal of Fluid Mechanics*, 210(501), 501-535.

Jones, E. N.; Sinclair, J. L. Effect of Solid Loading on Gas-Solid Flows. *AIChE J*., manuscript submitted.

Kameyama, K., Kanai, H., Kawashima & H., Ishima, T. (2014). *Evaluation of particle motion in solid-liquid two-phase pipe flow with downward/upward flow directions*, in: 17th Internatonal Symposium on Applications of Laser Techniques to Fluid Mechanics, 1–15.

Kasagi, N., & Shikazono, N. (1995). Contribution of Direct Numerical Simulation to Understanding and Modelling Turbulent Transport. *Proceedings: Mathematical and Physical Sciences*, 451(1941), 257-292.

Kenning, V.M., & Crowe C.T. (1997). On the effect of particle on carrier phase turbulence in gas-solid flow. *Int. J. Multiphase Flow*, 23 (2), 403–408.

Kiger, K., & Pan , C. (2002). Suspension and turbulence modification effects of solid particulates on a horizontal turbulent channel flow. *Journal of Turbulence*, 3(3), Journal of Turbulence, 01 January 2002, Issue 3.

Korving A.C. (2002). High concentrated fine-sand slurry flow in pipelines: an experimental study. *Hydrotransport* 15: BHR Group, Cran eld, UK; p. 769-776.

Krampa, F. (2009). *Two-fluid Modelling of Heterogeneous Coarse Particle Slurry Flows*. MSc Thesis, Department of Mechanical Engineering, University of Saskatchewan, Saskatoon, Canada

Krampa, F., Bergstrom, D., Bugg, J., Sanders, R., and Schaan, J. (2004). *Numerical simulation of dense coarse particle slurry flows in a vertical pipe*. In Matsumoto, Y., Hishida, K., Tomiyama, A., Mishima, K., and Hosokawa, S., editors, the 5th International Conference on Multiphase Flow, Yokohama, Japan. Proceedings on CD.

Laín, S., & Sommerfeld, M. (2008). Euler/Lagrange computations of pneumatic conveying in a horizontal channel with different wall roughness. *Powder Technology*, 184(1), 76-88.

Law, D., Battaglia, F., & Heindel, T. (2008). Model validation for low and high superficial gas velocity bubble column flows. *Chemical Engineering Science*, 63(18), 4605-4616.

Loth. E. (2011). *Particles, drops and bubbles: fluid dynamics and numerical methods*. Cambridge University Press, (in preparation, provided free and online).

Loulou, P., Moser, R., Mansour, N., & Cantwell, B. (1997). Direct numerical simulation of incompressible pipe flow using a B-spline spectral method. *NASA Technical Memo*. Data available at http://torroja.dmt.upm.es/ftp/AGARD/.

Louge, M., Mastorakos, E., & Jenkins, J. (1991). The role of particle collisions in pneumatic transport. *Journal of Fluid Mechanics*, 231, 345-359.

Lun, C. (2000). Numerical simulation of dilute turbulent gas–solid flows. *International Journal of Multiphase Flow*, 26(10), 1707-1736.

Lun, C., & Savage, S. (1987). *Kinetic Theory for Rapid Flow*; Department of Civil Engineering and Applied Mechanics, McGill University, Canada, unpublished manuscript.

Lun, C., & Savage, S. (2003). Kinetic Theory for Inertia Flows of Dilute Turbulent Gas-Solids Mixtures. In *Lecture Notes in Physics: Theory of Granular Gases*; Springer: New York; 267-289.

Lun, C., Savage, S., Jefferey, D., & Chepurniy, N. (1984). Kinetic theory for granular flow: Inelastic particles in Coutte flow and slightly inelastic particles in a general flowfield. *J. Fluid Mech*., 140, 223–256.

Lun, C., & Savage, K. (1986). The effects of an impact velocity dependent coefficient of restitution on stresses developed by sheared granular materials. *Acta Mechanica*, 63(1), 15-44.

Mandø, M., Lightstone, M., Rosendahl, L., Yin, C., & Sørensen, H. (2009). Turbulence modulation in dilute particle-laden flow. *International Journal of Heat and Fluid Flow*, 30(2), 331-338.

Matoušek, V. (2009). Predictive model for frictional pressure drop in settling-slurry pipe with stationary deposit. *Powder Technology*, 192(3), 367-374.

McKeon, B., Li, J., Jiang, W., Morrison, J., & Smits, A. (2004a). Further observations on the mean velocity distribution in fully developed pipe flow. *Journal of Fluid Mechanics*, 501(501), 135-147.

McKeon, B., Swanson, C., Zagarola, M., Donnelly, R., & Smits, A. (2004b). Friction factors for smooth pipe flow. *Journal of Fluid Mechanics*, 511, 41-44.

McKibben, M. (1992). *Wall Erosion in Slurry Pipelines*. PhD Thesis, Department of Chemical Engineering, University of Saskatchewan, Saskatoon, Canada.

Messa G. (2013), *Two-fluid model for solid-liquid flows in pipeline systems*, PhD in Environmental and Infrastructures Engineering (XXV cycle), Politecnico di Milano.

Messa, G., & Malavasi, S. (2014). Numerical prediction of dispersed turbulent liquid-solid flows in vertical pipes. *Journal of Hydraulic Research*, 52(5), 684-692.

Myong, H., & Kasagi, N. (1990). A New Approach to the Improvement of k-ε Turbulence Model for Wall-Bounded Shear Flows. JSME International Journal. Ser. 2, Fluids Engineering, Heat Transfer, Power, Combustion, Thermophysical Properties, 33(1), 63-72.

Ocone, Sundaresan, & Jackson. (1993). Gas-Particle flow in a duct of arbitrary inclination with particle-particle interactions. *AIChE Journal*, 39(8), 1261-1271.

Panneerselvam, R., Savithri, S., & Surender, G. (2009). CFD simulation of hydrodynamics of gas–liquid–solid fluidised bed reactor. *Chemical Engineering Science*, 64(6), 1119-1135.

Patankar, S. (1980). *Numerical heat transfer and fluid flow* (Series in computational methods in mechanics and thermal sciences). Washington : Toronto: Hemisphere Pub. ; McGraw-Hill.

Peirano, E. and Leckner, B. (1998). Fundamentals of turbulent gas-solid flows applied to circulating fluidized bed combustion. *Prog. Energy Combust*. Sci., 24, 259–296.

Pope, S. (2000). *Turbulent flows*. Cambridge ; New York: Cambridge University Press.

Rao, A., Curtis, J., Hancock, B., & Wassgren, C. (2012). Numerical simulation of dilute turbulent gas-particle flow with turbulence modulation. *AIChE Journal*, 58(5), 1381-1396.

Sanders, R., Ferre, A., Maciejewski, W., Gillies, R., & Shook, C. (2000). Bitumen effects on pipeline hydraulics during oil sand hydrotransport. *Canadian Journal of Chemical Engineering*, 78(4), 731-742.

Sato, Y., Hanzawa, A., Hishida, K., Maeda, M. (1995). Interaction between particle wake and turbulence in a water channel flow (PIV measurments and modelling for turbulence modification), in *Proceedings of the Second International Conference on Multiphase Flow*, edited by A. Serizawa, T. Fukano, and J. Bataille (Elsevier, Amsterdam), 27.

Schaan, J. (2001). *Pipeline flow of Newtonian fine particle slurries*. M.Sc. thesis, University of Saskatchewan, Saskatoon, Canada.

Schaeffer, D. (1987). Instability in the evolution equations describing incompressible granular flow. *Journal of Differential Equations*, 66(1), 19-50.

Sheen, H., Chang, Y., & Chiang, Y. (1993). Two-dimensional measurements of flow structure in a two-phase vertical pipe flow. *Proceedings of the National Science Council, Republic of China, Part A: Physical Science and Engineering*, 17(3), 200-213.

Sinclair, J., & Jackson, R. (1989). Gas-particle flow in a vertical pipe with particle-particle interactions. *AIChE Journal*, 35(9), 1473-1486.

Sinclair, J., & Mallo, T. (1998), *Describing Particle-Turbulence Interaction in a Two-Fluid Modelling Framework.* Proc. of ASME Fluids Engineering Division Summer Meeting (FEDSM'98), Washington, DC, June 21–25.

So, R., Zhang, H., & Speziale, C. (1991). Near-wall modeling of the dissipation rate equation. *AIAA Journal*, 29(12), 2069-2076.

Sommerfeld, M., & Kussin, J. (2004). Wall roughness effects on pneumatic conveying of spherical particles in a narrow horizontal channel. *Powder Technology*, 142(2-3), 180-192.

Spelay, R., Gillies, R., Hashemi, S., & Sanders, R. (2016). Effect of pipe inclination on the deposition velocity of settling slurries. *Canadian Journal of Chemical Engineering*, 94(6), 1032-1039.

Srivastava, A., & Sundaresan, S. (2003). Analysis of a frictional–kinetic model for gas–particle flow. *Powder Technology*, 129(1-3), 72-85.

Sumner, R.J., McKibben M.J., & Shook C.A. (1990). Concentration and velocity distributions in turbulent vertical slurry flows. *Ecoulements Solide Liquide*, 2 (2), 33–42.

Sumner, R. J. (1992). *Concentration Variations and Their Effects in Flowing Slurries and Emulsions*. PhD Thesis, Department of Chemical Engineering, University of Saskatchewan, Saskatoon, Canada.

Sun, B., & Gidaspow, D. (1999). Computation of circulating fluidized-bed riser flow for the Fluidization VIII benchmark test. *Industrial and Engineering Chemistry Research, 38*(3), 787-792.

Suzuki, Y., Ikenoya, M., & Kasagi, N. (1999). Simultaneous measurement of fluid and dispersed phases in a particle-laden turbulent channel flow with the aid of 3-D PTV. *International Workshop on Particle Image Velocimetry, 3rd, Santa Barbara, CA, 29*, S185-S193.

Tennekes, H., & Lumley, John L. (1972). *A first course in turbulence*. Cambridge, Mass., MIT Press.

Troshko, A., & Zdravistch, F. (2009). CFD modeling of slurry bubble column reactors for Fisher–Tropsch synthesis. *Chemical Engineering Science*, 64(5), 892-903.

Tsuji, Y. (2000). Activities in discrete particle simulation in Japan. *Powder Technology*, 113, 278–286.

Tsuji, Y., Kawaguchi, & Tanaka. (1993). Discrete particle simulation of two-dimensional fluidized bed. *Powder Technology*, 77(1), 79-87.

Tsuji, Y., Morikawa, Y., & Shiomi, H. (1984). LDV measurements of an air-solid two-phase flow in a vertical pipe. *Journal of Fluid Mechanics*, 139*,* 417-434.

Wang, X., Jia, X., & Wen, J. (2011). Transient CFD modeling of toluene waste gas biodegradation in a gas–liquid–solid three-phase airlift loop reactor by immobilized Pseudomonas putida. *Chemical Engineering Journal*, 172(2), 735-745.

Wen, C., and Yu, Y. (1966), Mechanics of Fluidization, *Chem. Eng. Prog. Symp*., 62, 100–111.

Wilcox, D. (2002). *Turbulence modeling for CFD* (2nd ed.). La Cañada, Calif.: DCW Industries.

Wu, C., Yan, B., Jin, Y., & Cheng, Y. (2010). Modeling and simulation of chemically reacting flows in gas–solid catalytic and non-catalytic processes. Particuology, 8(6), 525-530.

Wu, X., & Moin, P. (2008). A direct numerical simulation study on the mean velocity characteristics in turbulent pipe flow. *Journal of Fluid Mechanics*, 608, 81-112.

Yerrumshetty, A. (2007). *Numerical Prediction of Turbulent Gas-solid and Liquid-solid Flows Using Two-fluid Models*. . MSc Thesis, Department of Mechanical Engineering, University of Saskatchewan, Saskatoon, Canada

Zagarola, M., & Smits, A. (1998). Mean-flow scaling of turbulent pipe flow. *Journal of Fluid Mechanics*, 373, 33-79.

Zhang, Y., & Reese, J. (2001). Particle–gas turbulence interactions in a kinetic theory approach to granular flows. *International Journal of Multiphase Flow*, 27(11), 1945-1964.

Zhang, Y., & Reese, J. (2003). Gas turbulence modulation in a two-fluid model for gas–solid flows. *AIChE Journal*, 49(12), 3048-3065.

Zhao, Y., Ding, Y., Wu, C., & Cheng, Y. (2010). Numerical simulation of hydrodynamics in downers using a CFD–DEM coupled approach. *Powder Technology*, 199(1), 2-12.

Zhou, Z., Kuang, S., Chu, K., & Yu, A. (2010). Discrete particle simulation of particle-fluid flow: Model formulations and their applicability. *Journal of Fluid Mechanics*, 661, 482-510.

Zhu, H., Zhou, Z., Yang, R., & Yu, A. (2007). Discrete particle simulation of particulate systems: Theoretical developments. *Chemical Engineering Science*, 62(13), 3378-3396.

Zhuang, Y., Chen, X., Luo, Z., & Xiao, J. (2014). CFD–DEM modeling of gas–solid flow and catalytic MTO reaction in a fluidized bed reactor. *Computers and Chemical Engineering*, 60(C), 1-16.

Zaman, A., & Bergstrom, D. (2014). Implementation of Two-Fluid Model for Dilute Gas-Solid Flow in Pipes With Rough Walls. *Journal of Fluids Engineering*, 136(3), 031301/1-031301/11.

Zisselmar, R., & Molerus, O. (1979). Investigation of solid-liquid pipe flow with regard to turbulence modification. *The Chemical Engineering Journal*, 18(2), 233-239.

# APPENDIX

This appendix contains the algorithm flowchart of the in-house code used for performing numerical calculations in the present research work. The code is developed in FORTRAN and allows simulation of single-phase or multiphase flow, turbulent or laminar and in pipe or channel. The code gives flexibility to add additional features from different models by modifying specific sections of the code and declaring the respective new variables at the beginning.

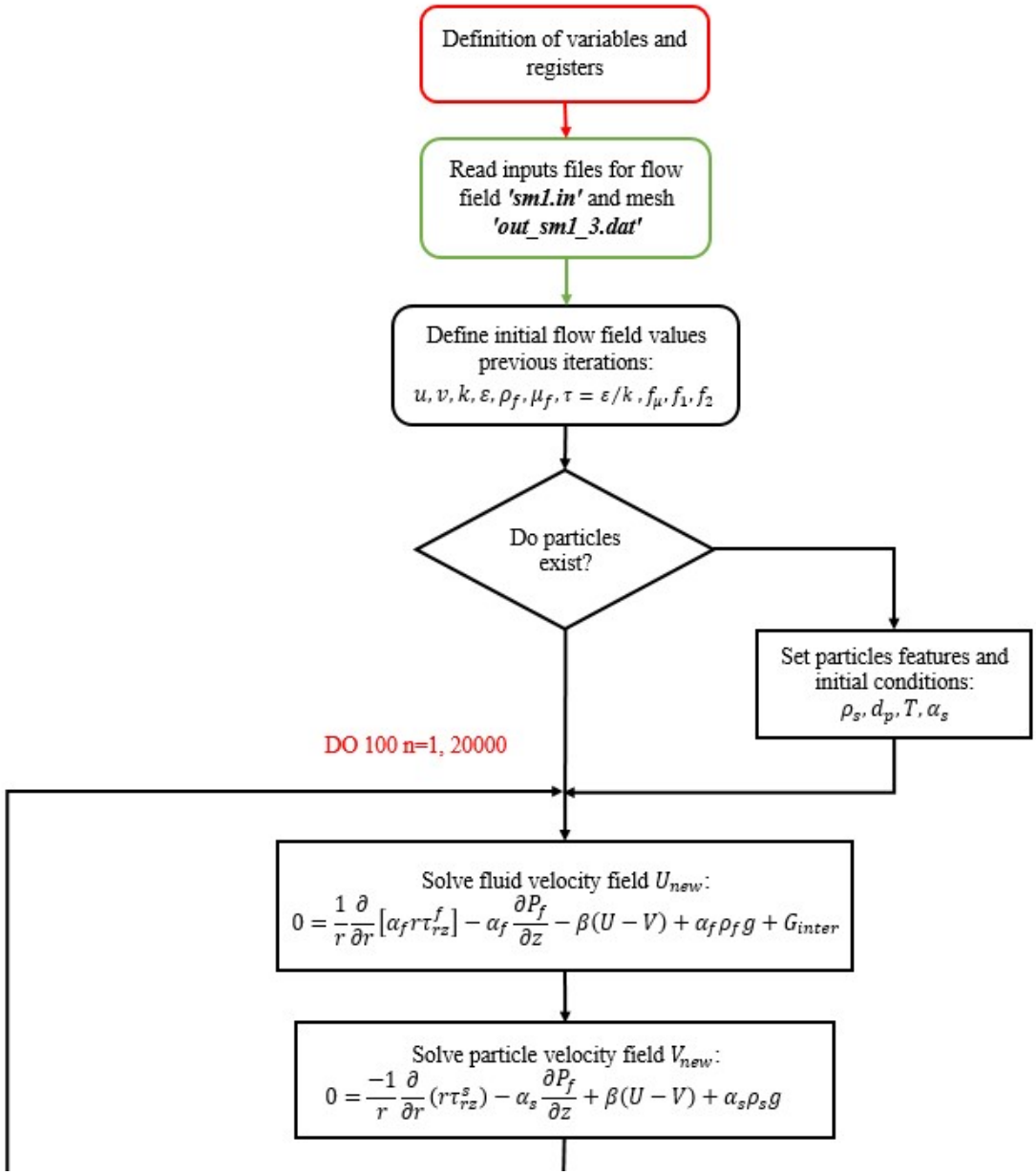

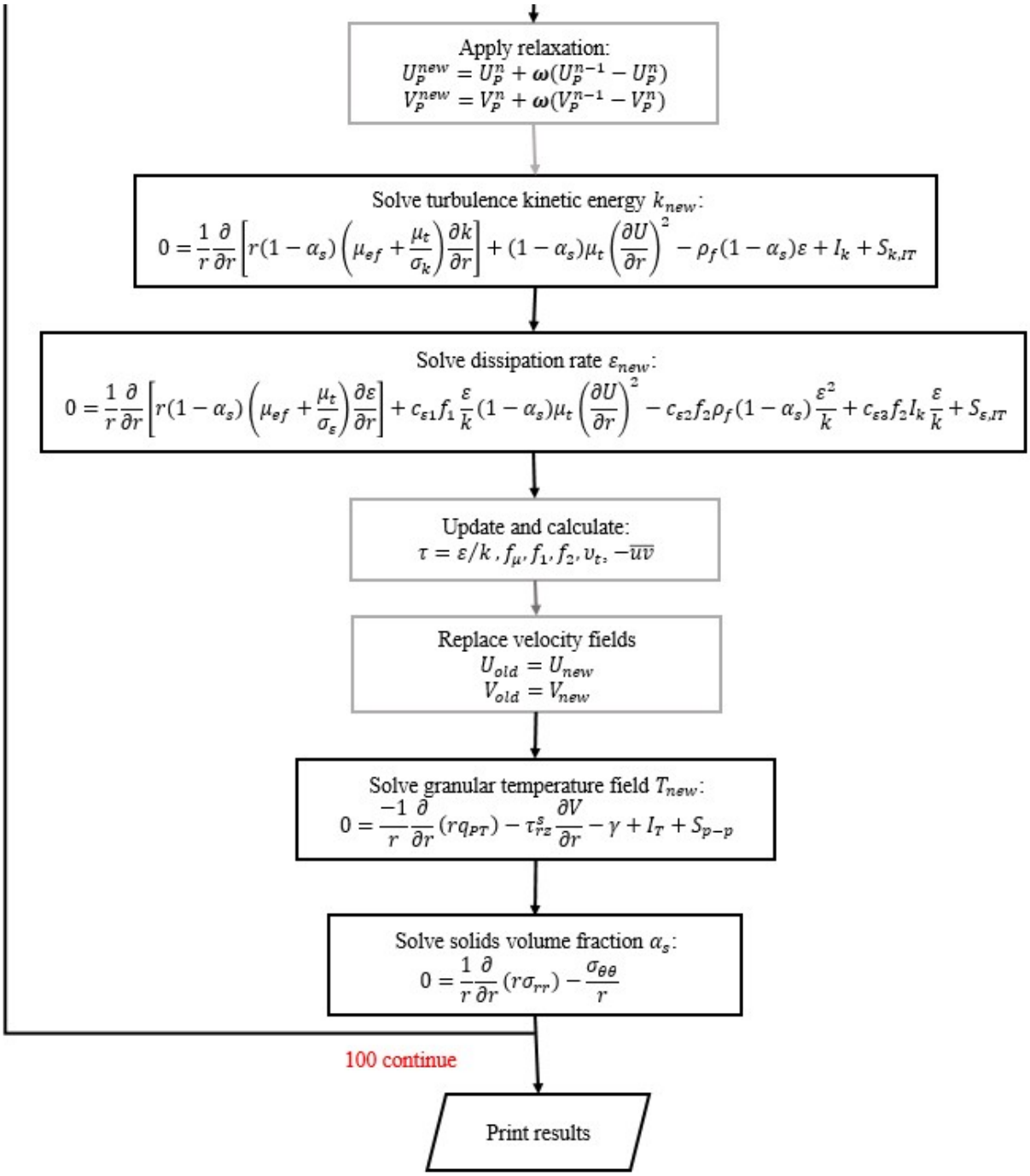


**Figure A.1:** In-house code algorithm flowchart.